Article

Neuron

Depression of Accumbal to Lateral Hypothalamic Synapses Gates Overeating

Highlights

- Following food restriction or during high-fat diet, mice overeat
- Overeating is mediated by synaptic depression at D1-MSN-to-LH inhibitory transmission
- Endocannabinoid signaling is necessary for the synaptic depression
- Synaptic potentiation at D1-MSN terminals in the LH prevents overeating

Authors

Sarah Thoeni, Michaël Loureiro, Eoin C. O'Connor, Christian Lüscher

Correspondence

christian.luscher@unige.ch

In Brief

Thoeni et al. identify a neural circuit adaptation that explains why mice overeat after food deprivation or when offered highly palatable chow. Endocannabinoids depress synapses between the nucleus accumbens and the lateral hypothalamus, opening the gate for excessive intake. Their findings may help to understand yo-yo dieting and obesity.

Thoeni et al., 2020, Neuron *107*, 1–15
July 8, 2020
https://doi.org/10.1016/j.neuron.2020.03.029

CellPress

Please cite this article in press as: Thoeni et al., Depression of Accumbal to Lateral Hypothalamic Synapses Gates Overeating, Neuron (2020), https://doi.org/10.1016/j.neuron.2020.03.029

Neuron
Article

Depression of Accumbal to Lateral Hypothalamic Synapses Gates Overeating

Sarah Thoeni,[1,3] Michaël Loureiro,[1,3] Eoin C. O'Connor,[1,3,4] and Christian Lüscher[1,2,5,*]
[1]Department of Basic Neuroscience, Faculty of Medicine, University of Geneva, Geneva, Switzerland
[2]Clinic of Neurology, Department of Clinical Neurosciences, Geneva University Hospital, Geneva, Switzerland
[3]These authors contributed equally
[4]Present address: Department of Neuroscience and Rare Diseases, Pharma Research & Early Development, F. Hoffmann-La Roche, Roche Innovation Center Basel, Basel, Switzerland
[5]Lead Contact
*Correspondence: christian.luscher@unige.ch
https://doi.org/10.1016/j.neuron.2020.03.029

SUMMARY

Overeating typically follows periods of energy deficit, but it is also sustained by highly palatable foods, even without metabolic demand. Dopamine D1 receptor-expressing medium spiny neurons (D1-MSNs) of the nucleus accumbens shell (NAcSh) project to the lateral hypothalamus (LH) to authorize feeding when inhibited. Whether plasticity at these synapses can affect food intake is unknown. Here, *ex vivo* electrophysiology recordings reveal that D1-MSN-to-LH inhibitory transmission is depressed in circumstances in which overeating is promoted. Endocannabinoid signaling is identified as the induction mechanism, since inhibitory plasticity and concomitant overeating were blocked or induced by CB1R antagonism or agonism, respectively. D1-MSN-to-LH projectors were largely non-overlapping with D1-MSNs targeting ventral pallidum or ventral midbrain, providing an anatomical basis for distinct circuit plasticity mechanisms. Our study reveals a critical role for plasticity at D1-MSN-to-LH synapses in adaptive feeding control, which may underlie persistent overeating of unhealthy foods, a major risk factor for developing obesity.

INTRODUCTION

Metabolic need drives feeding via the action of peripheral and central signals converging onto brain areas involved in food seeking and consumption (Burnett et al., 2016; Ferrario et al., 2016; Morton et al., 2014; Sohn et al., 2013). For example, periods of caloric deficit can drive compensatory eating through the release of hormones, including leptin and insulin, recruiting mesolimbic and hypothalamic brain circuitry (Hambly and Speakman, 2015; Mebel et al., 2012; O'Connor et al., 2016; Penicaud and Le Magnen, 1980). This physiological response ensures the refill of energy stores, but it can lead to difficulties in sustaining reductions in body weight following diets based solely on caloric restriction or fasting (Hall and Kahan, 2018; Rosenbaum et al., 2010). Conversely, eating can occur in the absence of immediate metabolic need, such as when faced with highly palatable and energy-dense foods. With these foods readily available in many societies, eating despite satiety is considered a key factor underlying weight gain and obesity (Berridge, 2009; Morris et al., 2015). The current means to limit excess feeding and obesity are few and often fail to support the long-term maintenance of reduced body weight (Hall and Kahan, 2018). Thus, a better understanding of mechanisms that regulate brain circuits involved in eating and overeating will be crucial to identify novel treatments.

Hypothalamic nuclei are well described for their role in feeding regulation and energy homeostasis (Varela and Horvath, 2012; Waterson and Horvath, 2015). The lateral hypothalamic area (LH) controls food intake via the activity of a heterogeneous cell population expressing orexigenic and anorexigenic neuropeptides and classical neurotransmitters (Arrigoni et al., 2019; Bonnavion et al., 2016; Petrovich, 2018; Stuber and Wise, 2016). For example, LH neurons expressing either γ-aminobutyric acid (GABA) or glutamatergic markers have been found to support or suppress food intake, respectively (Jennings et al., 2013, 2015; Nieh et al., 2016; Stamatakis et al., 2013).

A major source of inhibitory control over LH arises from medium spiny neurons that express the dopamine D1 receptor (D1-MSNs) and whose cell bodies are located in the nucleus accumbens shell (NAcSh) (O'Connor et al., 2015). Acute inhibition of NAcSh activity, achieved by the blockade of glutamate transmission or the stimulation of $GABA_A$ receptors elicits robust food intake (Maldonado-Irizarry et al., 1995; Urstadt et al., 2013; Will et al., 2003), in addition to stimulation of the opioid or endocannabinoid system (Peciña and Berridge, 2005; Soria-Gómez et al., 2007). These effects are mediated in part via a disinhibition of LH (Stratford and Kelley, 1999; Urstadt et al., 2013). Consistent with these pharmacological manipulations, it is found through *in vivo* electrophysiological recordings that accumbal D1-MSN activity is reduced during feeding (Krause et al., 2010; O'Connor et al., 2015), and brief electrical stimulation of NAcSh or optogenetic activation of D1-MSN projections to LH is sufficient to abruptly stop food intake (O'Connor et al., 2015; Krause et al., 2010). These findings support a model in which the reduced activity of NAcSh D1-MSNs disinhibits LH neurons to authorize food intake (O'Connor et al., 2015).

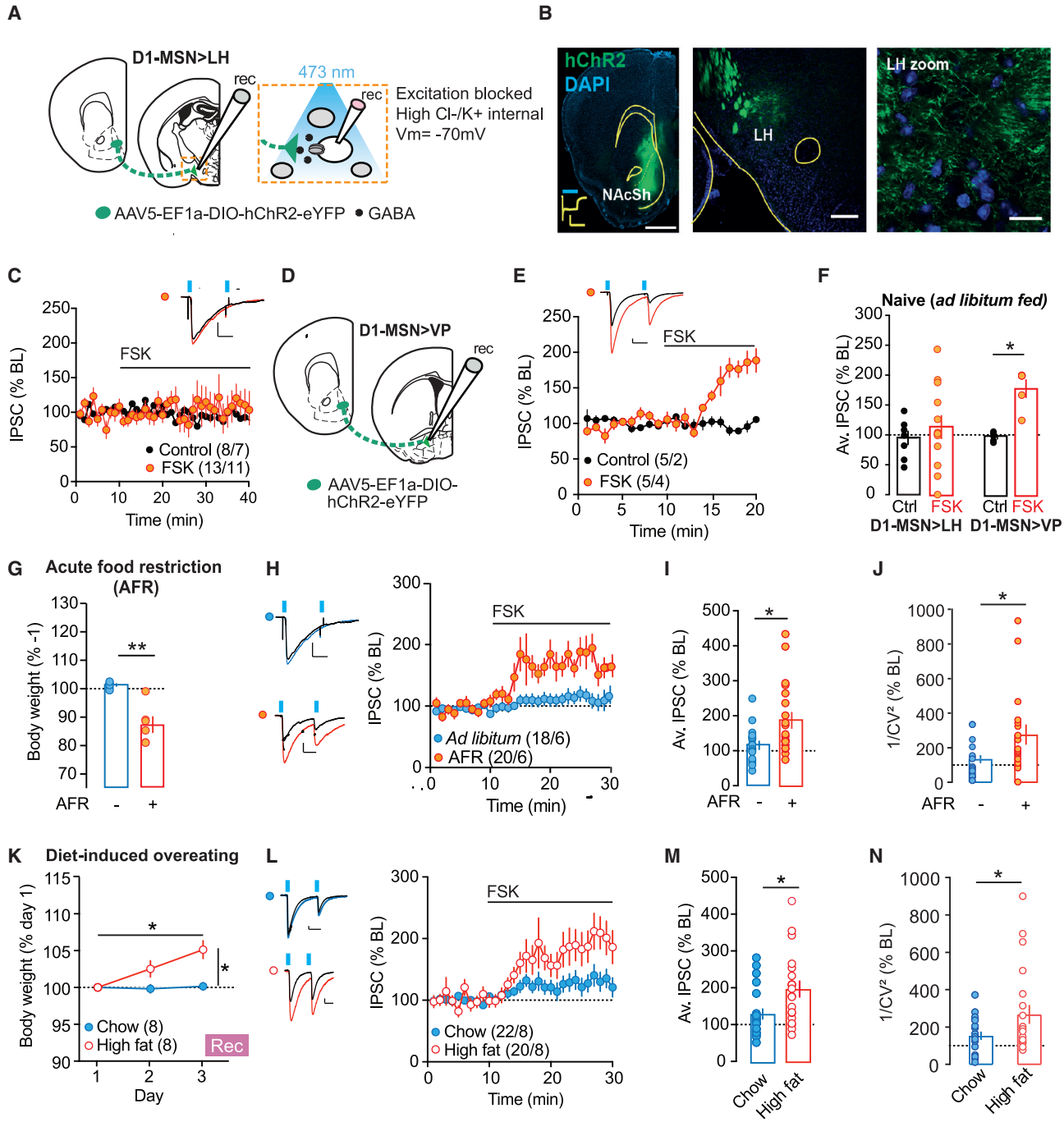

Figure 1. D1-MSN-to-LH Plasticity Is Revealed after Food Restriction or High-Fat Diet

(A) Schematic of the preparation used for whole-cell patch clamp recordings.

(B) Left: representative image of NAcSh ChR2 transfection and example trace of 500-ms blue light-evoked photocurrent from ChR2-expressing neuron (scale: 500 pA, 500 ms, 1 mm). Center: representative image of LH with ChR2-EYFP-labeled fiber terminals originating from NAcSh at low (scale bar: 200 μm) and (right) high magnification (scale bar: 20 μm).

(C) Normalized IPSCs for bath application of forskolin (FSK; 10 μM).

(D) Schematic for NAcSh-to-VP recordings.

(E) Same as in (C), but at NAcSh-to-VP synapses.

(F) Average norm. IPSC from last 5 min of recordings for cells recorded in LH and VP. At D1-MSN-to-LH synapses, there was no change in IPSCs. ANOVA: treatment $F(1,34) = 6.899$, $p < 0.05$, region × treatment $F(1,34) = 3.781$, $p = 0.06$. At D1-MSN-to-VP synapses, FSK application significantly increased IPSCs versus controls. *Unpaired t test, $t34 = 2.664$, $p < 0.05$.

(legend continued on next page)

While the moment-to-moment control over food intake mediated by the activity of NAcSh D1-MSN-to-LH projections is relatively well established, little is known about long-lasting adaptive changes. An appealing hypothesis would be the contribution of synaptic plasticity in this circuit. Plasticity mechanisms could provide a powerful way to regulate feeding over a longer timescale wherein reduced synaptic strength of the NAcSh-to-LH pathway would be predicted to promote food intake, while, conversely, increased synaptic strength would tightly constrain feeding. Synaptic plasticity of inhibitory transmission at accumbal D1-MSN projections to the ventral tegmental area (VTA) and ventral pallidum (VP) have been described (Bocklisch et al., 2013; Creed et al., 2016), but whether this plasticity is also present at the D1-MSN-to-LH synapse is not known. Notably, a prior study reported the persistent reduction of feeding after deep-brain stimulation (DBS) of the NAcSh, together with a decreased firing rate of LH neurons (Wei et al., 2015), suggesting that long-term changes in synaptic transmission in the NAcSh-to-LH pathway had occurred. We therefore sought to characterize plasticity at NAcSh-to-LH synapses and understand its relevance for feeding control.

Herein, synaptic transmission was assessed using electrophysiological recordings in *ex vivo* brain slices of mice, taking advantage of optogenetic and genetic tools to stimulate and record from identified NAcSh and LH neuronal populations. Unlike D1-MSN-to-VP or -VTA synapses (Bocklisch et al., 2013; Creed et al., 2016), inhibitory plasticity induced by high-frequency stimulation or adenylyl cyclase activation at D1-MSN-to-LH synapses was absent in naive *ad libitum*-fed animals. Neural tracing studies identified D1-MSN-to-LH projections as largely non-overlapping with D1-MSN-to-VP or -VTA projections, providing an anatomical basis for this observation. Instead, after manipulations leading to increased feeding (i.e., acute food deprivation, exposure to high-calorie food), adenylyl cyclase activation caused the potentiation of inhibitory transmission at this synapse, revealing a depression during overeating. Endocannabinoid signaling was identified as the mechanism underlying the depression in synaptic transmission, as the blockade of cannabinoid type 1 receptors (CB1Rs) was sufficient to prevent compensatory feeding following acute food restriction, weight gain following high-fat diet exposure, and the associated plasticity. Conversely, CB1R activation induced an inhibitory depression at D1-MSN-to-LH synapses in *ad libitum*-fed animals and was sufficient to increase feeding in this condition when infused locally into LH. Finally, *in vivo* high-frequency stimulation of D1-MSN terminals in the LH reduced consumption in food-restricted mice. Our results support a model in which increased feeding is promoted through endocannabinoid-dependent synaptic depression of accumbal D1-MSN-to-LH synapses.

RESULTS

D1-MSN-to-LH Plasticity Is Revealed When Overeating Is Favored

In naive mice, accumbal D1-MSN-to-VP and -VTA synapses undergo a form of inhibitory long-term potentiation (i-LTP) in response to the activation of adenylyl cyclase with forskolin (FSK; Bocklisch et al., 2013; Creed et al., 2016). We assessed whether NAcSh D1-MSN-to-LH synapses were susceptible to i-LTP induced by the same protocol. Adult male and female D1cre mice were injected with an adeno-associated virus (AAV) to express a floxed channelrhodopsin-2 construct (AAV5-DIO-EF1A-ChR2(H134R)-EYFP) in the NAcSh (Figures 1A and 1B). Approximately 1 month later, acute brain slices were prepared to record from LH neurons using whole-cell patch clamp electrophysiology. Inhibitory postsynaptic currents (IPSCs) at NAcSh D1-MSN-to-LH synapses were elicited with brief, blue light pulses. FSK (10 μM) could not induce i-LTP at the NAcSh D1-MSN-to-LH synapse (Figure 1C). However, in the same preparation but recording instead from VP neurons while optogenetically stimulating D1-MSN terminals, the application of FSK reliably induced i-LTP from all of the cells recorded (Figures 1D–1F). Hence, these data indicate that in naive *ad libitum*-fed mice, i-LTP of the NAcSh D1-MSN-to-LH synapse is absent, and this finding is distinct from other major target nuclei of accumbal D1-MSNs (Bocklisch et al., 2013; Creed et al., 2016).

At some synapses, plasticity is activity dependent and only revealed after exposure to a specific stimulus (Wamsteeker Cusulin et al., 2013; Inoue et al., 2013). Given the importance of the NAcSh-to-LH pathway in controlling food intake, we wondered whether a change in synaptic transmission would be revealed following exposure to a manipulation that would drive increased feeding or overeating. To this end, D1Cre mice transfected with floxed-ChR2 in the NAcSh were subject to acute food restriction (AFR) overnight and sacrificed the following morning to assess plasticity at the D1-MSN-to-LH synapse *ex vivo*. As expected, AFR led to a significant reduction in body weight as compared to *ad libitum*-fed controls (Figure 1G). Consistent with the

(G) D1Cre mice with floxed-ChR2 in NAcSh were food restricted overnight (AFR) and plasticity at D1-MSN-to-LH synapse was assessed the next day. Body weight (% day 1) was significantly reduced in AFR mice versus *ad libitum*-fed controls. **Unpaired t test, $t10 = -4.97$, $p < 0.01$.

(H) Normalized IPSCs for FSK applied in AFR or *ad libitum*-fed mice.

(I) Mean norm. IPSC from last 5 min of recordings following FSK is significantly increased in AFR mice versus controls. *Unpaired t test, $t36 = 2.72$, $p < 0.05$.

(J) Coefficients of variation of the amplitude of the IPSCs were increased after FSK $t35 = 2.309$, $*p < 0.05$.

(K) Body weight significantly increased in mice fed high-fat diet over 3 days, compared to mice with access only to chow. ANOVA: diet × time interaction: $F(2,18.9) = 10.2$, $p < 0.01$. High-fat diet versus chow, unpaired t test at day 3, $t14 = 3.78$, $p < 0.01$; for high-fat diet, day 3 versus day 1, paired t test, $t7 = 85.7$, $p < 0.01$.

(L) Norm. IPSCs before and after application of FSK.

(M) Average IPSC (% of baseline [BL]) from the last 5 min of recordings. The average IPSC (% BL) was significantly increased in mice exposed to high-fat diet versus chow. *Unpaired t test, $t40 = 2.69$, $p < 0.05$.

(N) Coefficients of variation of the amplitude of the IPSCs were increased in the high-fat diet group. $t40 = 2.063$, $*p < 0.05$.

Plots show means ± SEMs. $*p < 0.05$, $**p < 0.01$.

Scale bars for (C), (D), (F), and (I): 50 pA, 20 ms.

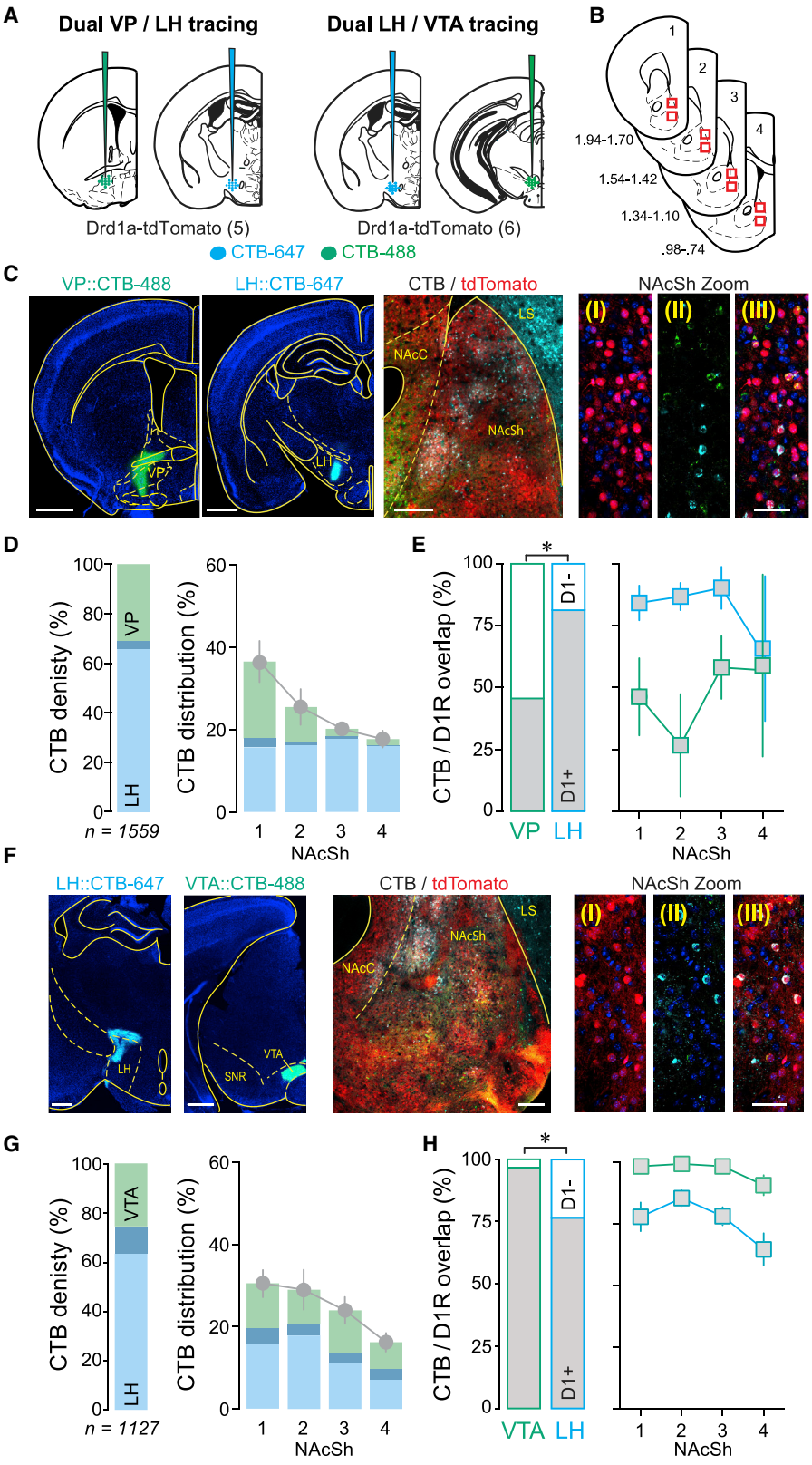

(legend on next page)

previous experiment, the D1-MSN-to-LH synapse did not show any plasticity upon bath application of FSK onto slices from control animals. Instead, in slice from food-restricted mice, FSK application now led to a robust potentiation of inhibitory transmission at the D1-MSN-to-LH synapse (Figures 1H and 1I). FSK-induced i-LTP was absent 1 week after AFR at a time when body weight loss had recovered (Figure S1), indicating that synaptic depression of D1-MSN-to-LH synapses is present only in situations that favor overeating (i.e., after AFR).

Previous studies have found that inhibitory plasticity at D1R-MSN projection terminals requires the presynaptic activation of protein kinase A and D1 receptors to induce i-LTP (Bocklisch et al., 2013; Creed et al., 2016). Specifically, at D1-MSN projections to the VP or VTA, the presynaptic expression locus was confirmed by a change in the variance of inhibitory currents ($1/CV^2$; Bocklisch et al., 2013; Creed et al., 2016). Likewise, in our recordings, the variance of inhibitory currents also increased after FSK application in AFR mice (Figure 1J), again pointing to a presynaptic expression locus.

Overeating can also occur in the absence of any immediate metabolic need—for example, when exposed to highly palatable and calorically dense foods, particularly those rich in fats or sugars (Morton et al., 2014). Would increased feeding of energy dense, high-fat diet recruit plasticity at the D1-MSN-to-LH synapse? To answer this question, D1cre mice transfected with floxed-ChR2 in the NAcSh were provided exclusively with a high-fat diet in their home cage. Control D1cre mice received normal chow. Three days of feeding was sufficient to produce increased weight gain in mice fed a high-fat diet as compared to chow-fed controls (Figure 1K). After 3 days of feeding, acute brain slices of LH were prepared for *ex vivo* recordings as per previous experiments. As expected, chow-fed control mice did not demonstrate potentiation of the D1-MSN-to-LH synapse upon FSK application. On the contrary, in LH slices from high-fat-fed mice, the amplitude of IPSCs at this synapse was significantly increased following FSK application (Figures 1L and 1M). The IPSC variance changed at cells recorded from high-fat diet-exposed mice (Figure 1N), suggesting that high-fat food exposure also changed the release probability at D1-MSN-to-LH synapses. These data show that divergent stimuli (food-restriction or high-fat diet) that both favor overeating lead to plasticity at the D1-MSN-to-LH synapse.

NAcSh D1-MSN-to-LH Projectors Are Segregated from D1-MSN-to-VP or -VTA Projections

Accumbal MSNs provide dense inhibition to various downstream nuclei, including the VP, LH, and VTA, with each target ascribed distinct behavioral functions (Bocklisch et al., 2013; Creed et al., 2016; Gibson et al., 2018; O'Connor et al., 2015; Pardo-Garcia et al., 2019). However, whether individual D1-MSNs target these output nuclei in an exclusive or overlapping manner is not fully understood (Pardo-Garcia et al., 2019). To address this question, a dual retrograde tracing strategy was applied using region-specific injections of cholera toxin subunit B (CTB) coupled to Alexa fluorophors in Drd1a-tdTomato mice to allow the reliable identification of D1-MSNs.

The first cohort of mice (n = 5) was injected in the LH and VP with equal volumes of CTB-647 or CTB-488, respectively (Figure 2A). Eleven days after the injections, coronal slices containing NAcSh from four points along its rostro-caudal axis were prepared (Figure 2B). Although we cannot exclude that damaged fibers of passage may uptake CTB, a careful histological analysis shows minimal injection lesions in the LH (Figure S2), which is in line with only a few cells that showed overlapping expression of both CTB tracers. Slices were imaged via confocal microscopy (2× [320 × 320 μm] images per section) and analyzed for the expression of the 2 CTB tracers, together with tdTomato (Figure 2C). A total of 1,559 CTB-labeled neurons were identified from all of the NAcSh images (Figure 2D). NAcSh-to-LH projectors comprised 69.2% ± 3.8% of all CTB-labeled cells, while 34.4% ± 3.9% of cells were identified as NAcSh-to-VP projectors. Only 3.6% ± 1.0% of labeled cells expressed both CTB fluorophores, suggesting little overlap between NAcSh-to-LH and -VP projectors (Figure 2D). Analysis of CTB and tdTomato colocalization confirmed prior reports that accumbal projections to VP comprise both D1- and non-D1- (i.e., D2-) expressing MSNs in roughly equal proportions (45.6% ± 6.94% were identified as D1-MSNs; Figure 2E) (Creed et al., 2016; Kupchik et al., 2015), while 81.3% ± 4.3% of

Figure 2. D1-MSN-to-LH Projectors Are Segregated from D1-MSN-to-VP or -VTA Projections

(A) Schematic of preparation. CTBs were injected in the VP and LH (for C–E) or VTA and LH (for F–H) of Drd1a-tdTomato mice.

(B) Schematic of sites imaged for quantification across the rostro-caudal gradient of NAcSh.

(C) Left: example images of CTB injection sites in VP and LH. Scale bar: 1,000 μm. Center: example image of NAcSh showing D1-MSNs labeled by tdTomato, and CTB-labeled cells from VP and LH. Scale bar: 200 μm. Right: representative images of NAcSh in high magnification: (I) D1-MSNs labeled by tdTomato; (II) VP and LH projectors labeled with CTB-488 and CTB-647, respectively; (III) merge. Scale bar: 50 μm.

VP and LH projectors identified by CTB-488 and CTB-647, respectively, Right: merge. Scale bar: 50 μm.

(D) Left: proportion of all CTB-labeled cells identified as LH (34.4% ± 3.9%) or VP (69.2% ± 3.8%) projectors, or cells expressing both fluorophores (3.6% ± 1.0%), Right: distribution of CTB-labeled cells across NAcSh rostro-caudal gradient (positions 1–4 refer to coordinates shown in B).

(E) Left: quantification of NAcSh-to-VP or -LH projectors also identified as D1-MSNs. 45.6% ± 6.9% of NAcSh-to-VP projectors were D1-MSNs, while significantly more LH projectors were D1-MSNs (81.3% ± 4.3%; paired t test, *$p < 0.05$). Right: proportion of CTB cells identified as D1-MSNs distributed across NAcSh rostro-caudal gradient.

(F) Same as for (C) but with CTB injections made in VTA or LH. Left: example images of CTB injection sites in LH and VTA. Scale bar: 1,000 μm. Center: example image of NAcSh showing D1-MSNs labeled by tdTomato, and CTB-labeled cells from LH and VTA. Scale bar: 100 μm. Right: representative images of NAcSh in high magnification: (I) D1-MSNs labeled by tdTomato; (II) LH and VTA projectors labeled with CTB-488 and CTB-647, respectively; (III) merge. Scale bar: 50 μm.

(G) Left: proportion of all CTB-labeled cells identified as LH (63.6% ± 3.2%) or VTA (47.5% ± 3.1%) projectors, or cells expressing both fluorophores (11.1% ± 1.2%), Right: distribution of cells across NAcSh rostro-caudal gradient.

(H) Left: quantification of NAcSh-to-VTA or -LH projectors also identified as D1-MSNs. 96.6% ± 2.0% of NAcSh-to-VTA projectors were D1-MSNs, while significantly fewer LH projectors were D1-MSNs (76.5% ± 4.3%; *paired t test, $p < 0.05$). Right: proportion of VTA or LH projectors identified as D1-MSNs distributed across NAcSh rostro-caudal gradient. Plots show means ± SEMs.

NAcSh-to-LH projectors were D1-MSNs (Figure 2E) (O'Connor et al., 2015). The few non-D1 projectors to LH (i.e., putative D2-MSNs) appeared to be more often found in the most caudal aspect of NAcSh (Figure 2E). Dual CTB tracing experiments were repeated in a second cohort of Drd1a-tdTomato mice, but now with LH and VTA injections of CTB-488 or CTB-647, respectively (n = 6; Figures 2A and 2F). From a total of 1,127 CTB-labeled cells in NAcSh, 63.6% ± 3.2% were projecting to the LH, 47.5% ± 3.1% to the VTA, and only 11.1% ± 1.2% to both structures (Figure 2G). CTB-labeled cells from the LH and VTA projectors were evenly distributed across NAcSh (Figure 2G), while colocalization analysis between CTB and tdTomato again confirmed prior studies in which the vast majority (96.6% ± 2.0%) of NAcSh-to-VTA projectors were D1-MSNs (Bocklisch et al., 2013; Yang et al., 2018), while 76.5% ± 4.3% of NAcSh-to-LH projectors were D1-MSNs (O'Connor et al., 2015). As for the LH-VP dual tracing experiment, putative D2-MSN-to-LH projectors tended to be more frequently found in the most caudal aspect of NAcSh (Figure 2H). Data from these two tracing studies demonstrated that NAcSh-to-LH projectors were largely non-overlapping with -VP and -VTA projectors, providing an anatomical basis for the distinct plasticity seen at these synapses.

An additional observation from these tracing studies was that D1-MSN innervation appeared to become gradually more dominant as the downstream target was located progressively more distally from NAcSh. To further explore this finding, we conducted one final dual retrograde tracing experiment in Drd1a-tdTomato mice, now with CTB-488 or CTB-647 injections made in anterior or posterior aspects of LH (aLH and pLH), respectively, in the same mouse (Figures S3A and S3B). From 3,219 CTB-labeled cells identified in NAcSh (n = 10 mice), 46.1% ± 8.1% projected to aLH, 67.9% ± 6.7% projected to pLH, and 13.9% ± 2.9% were identified as overlapping (Figure S3C). Again, aLH and pLH projectors were distributed evenly over the rostro-caudal extent of NAcSh (Figure S3C). Notably, while D1-MSNs formed the dominant projection for both aLH and pLH, there were significantly more D1-expressing cells projecting to pLH than to aLH (89.5% ± 0.7% versus 80.9% ± 3.5%, paired t test $p < 0.05$; Figure S3D). The few putative D2-MSN projectors to aLH and pLH were more often found in the caudal aspect of NAcSh (Figure S3D). Thus, our study reveals that D2-MSN innervation is progressively lost as accumbal projections extend to more distal targets and, across this same gradient, D1-MSN innervation comes to dominate.

Food Restriction Induces i-LTD onto Both LH Glutamatergic and GABAergic Neuronal Subpopulation

Synaptic plasticity can be critically dependent on the postsynaptic cell identity (Castillo et al., 2011). One possibility is that i-LTP was present in a subset of LH neurons but masked in the first experiment when recordings were made from non-identified and potentially heterogeneous cells types. Our prior work identified LH neurons expressing the vesicular GABA transporter (VGAT) as a target of NAcSh D1-MSN inhibition (O'Connor et al., 2015). *Ex vivo* plasticity experiments were therefore repeated, but now with selective recording of IPSCs from NAcSh-to-LH VGAT neurons (Figure 3). This was accomplished by transfecting the LH of VGATCre mice with an AAV expressing a fluorescent reporter protein in a floxed construct (AAV5-DIO-EF1A-mCherry), while NAcSh was transfected with non-floxed ChR2 (AAV5-hSyn-ChR2(H134R)-EYFP; Figure 3A). However, FSK-induced iLTP at NAcSh-to-LH VGAT synapses was revealed only in food-restricted animals (Figure 3B). Current variance increased in AFR mice following FSK application on slice (Figure 3C).

During these recordings, it became evident that LH neurons not expressing VGAT also received monosynaptic inhibition from NAcSh. A large population of LH neurons expresses the vesicular glutamate transporter-2 (VGluT2) and was also found to influence food intake, albeit in a directionality opposite that of LH VGAT neurons (Jennings et al., 2013). To assess whether LH VGluT2 neurons were also a target of D1R-MSN inhibition, Drd1a-tdTomato mice were crossed with VGluT2Cre mice to permit monosynaptic retrograde rabies tracing from LH VGluT2 neurons, with the identification of D1-MSNs via tdTomato expression (Figures 3D–3F) (Watabe-Uchida et al., 2012). Using this approach, MSNs that projected monosynaptically to LH VGluT2 neurons were revealed by EGFP labeling in NAcSh. Of these EGFP-labeled neurons, 97% (43 of 44 cells, n = 2 mice) were also positive for tdTomato, confirming their identity as D1-MSNs (Figure 3F). The functionality of the D1-MSN-to-LH VGluT2 neuron connection was then assessed by *ex vivo* recordings from fluorescently labeled LH VGluT2 neurons of VGluT2Cre mice, while monitoring bluelight-evoked IPSCs from ChR2-transfected NAcSh projections (Figures 3G–3I). Of all of the LH VGluT2$^+$ neurons recorded, 65% (28 of 43 cells, n = 5 mice) received inhibition from putative NAcSh D1-MSNs (Figure 3G). We then asked whether i-LTP could be induced at the NAcSh-to-LH VGluT2 synapse in naive or AFR mice. Similar to recordings performed in VGATcre mice, bath application of FSK induced i-LTP only in AFR mice (Figures 3H and 3I). These results identify a subpopulation of LH VGluT2 neurons that receive monosynaptic inhibition from NAcSh D1-MSNs. Irrespective of the postsynaptic LH neuron identity (non-identified, VGAT$^+$, or VGluT2$^+$), plasticity at D1-MSN-to-LH synapses was absent in naive animals but revealed by FSK in food-restricted animals. These findings provide further evidence for a presynaptic expression locus of the plasticity, which is largely blind to the postsynaptic target. Thus, in *ad libitum*-fed conditions, i-LTP at D1-MSN-to-LH synapses may already be occluded. A behavioral stimulus, in this case, AFR, leads to a weakening of synaptic strength (i.e., a long-term depression [LTD]) and only then can i-LTP be revealed by FSK.

CB1R Signaling Is Required for D1-MSN-to-LH Plasticity after Acute Food Restriction

What mechanism might be responsible for inducing i-LTD at D1-MSN-to-LH synapse during acute food restriction? A promising candidate is signaling at CB1Rs. CB1Rs are expressed by striatal MSNs (Martín et al., 2008), their activation leads to LTD via Gi/o-coupling (Atwood et al., 2014a, 2014b; Pertwee, 2006), and their role in feeding via actions on accumbens circuitry has been well established by microinfusion studies (Cortés-Salazar et al., 2014; Soria-Gómez et al., 2007; Tandon et al., 2017; Will et al., 2003; Zhang and Kelley, 2000).

To assess the effect of CB1R activation on D1-MSN-to-LH plasticity, brain slices containing LH were first prepared from *ad libitum*-fed D1Cre mice previously injected with floxed-ChR2

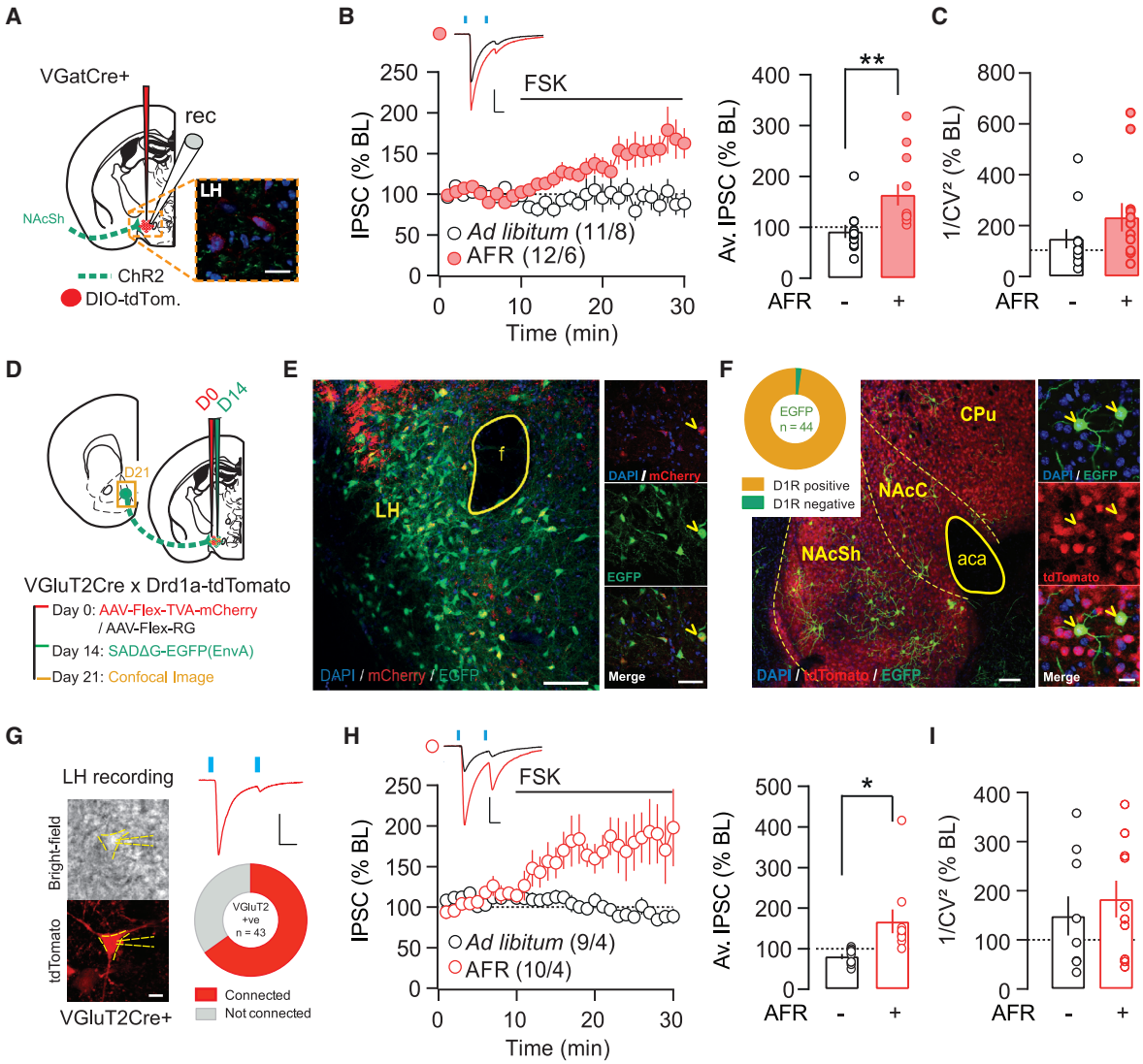

Figure 3. Food Restriction Induces i-LTD onto Both LH GABA and VGluT2 Neuronal Subpopulation

(A) Schematic of the preparation to investigate synaptic transmission onto LH VGat-expressing neurons, with example image of ChR2$^+$ NAc terminals (green) and VGat$^+$ neurons (red) in the LH (scale bar: 20 μm).

(B) Left: norm. IPSCs before and after application of FSK. Right: average IPSC (% BL) from the last 5 min of recordings. The average IPSC (%BL) was significantly increased in food-restricted mice. Unpaired t test, $t(21) = 2.91$, $p < 0.01$.

(C) Coefficients of variation of the amplitude of the IPSCs tend to increase in food-restricted animals but were not statistically significant. $t21 = 1.226$, $p = 0.23$.

(D) Schematic showing timeline of rabies-tracing experiment in Drd1a-tdTomato × VGluT2Cre mice.

(E) Low-magnification image of LH showing distribution of starter cells (expressing mCherry and GFP) and local pre-synaptic inputs expressing EGFP alone. Dense fibers in upper left corner likely reflect tdTomato expression from striatal projections, since tdTomato is not expressed in LH cell bodies (O'Connor et al., 2015). Scale bar: 50 μm. Panels at right show example starter cell, indicated by arrowhead. Scale bar: 50 μm.

(F) Low-magnification image of LH VGluT2 pre-synaptic cells in accumbens (left; scale bar: 100 μm), with panels exemplifying 2 neurons co-expressing EGFP and tdTomato (right; scale bar: 20 μm; i.e., D1R-MSNs monosynaptically projecting to LH VGLuT2 cells). CPu, caudate putamen; NAcC, accumbens core; NAcSh, accumbens shell; aca, anterior commissure. Inset shows the quantification of EGFP colocalization with tdTomato in accumbens; 43 of 44 accumbal cells projecting to LH VGLuT2 neurons were D1R-MSNs (n = 2 mice).

(G) Example recording from a connected VGluT2 neuron in response to blue light stimulation (2 × 4-ms light pulse, 50-ms interval). Summary connectivity plot showing 65% of VGluT2 neurons received light-evoked IPSCs from NAcSh afferents (28 of 43 cells; n = 5 mice). Scale bar: 20 ms, 200 pA.

(H) Left: norm. IPSCs before and after application of FSK. Right: average IPSC (% BL) from the last 5 min of recordings. The average IPSC (%BL) was significantly increased in food-restricted mice. Unpaired t test, $t(17) = 2.725$, $p < 0.05$.

(I) Coefficients of variation of the amplitude of the IPSCs in VGLUT$^+$ cells were not affected by food restriction. $t17 = 0.63$, $p = 0.54$. Representative traces show a mean of 30 sweeps during baseline (black) and at the end of recording (red), after FSK application. Scale bars: 50 pA, 20 ms. Plots show means ± SEMs. *$p < 0.05$, **$p < 0.01$.

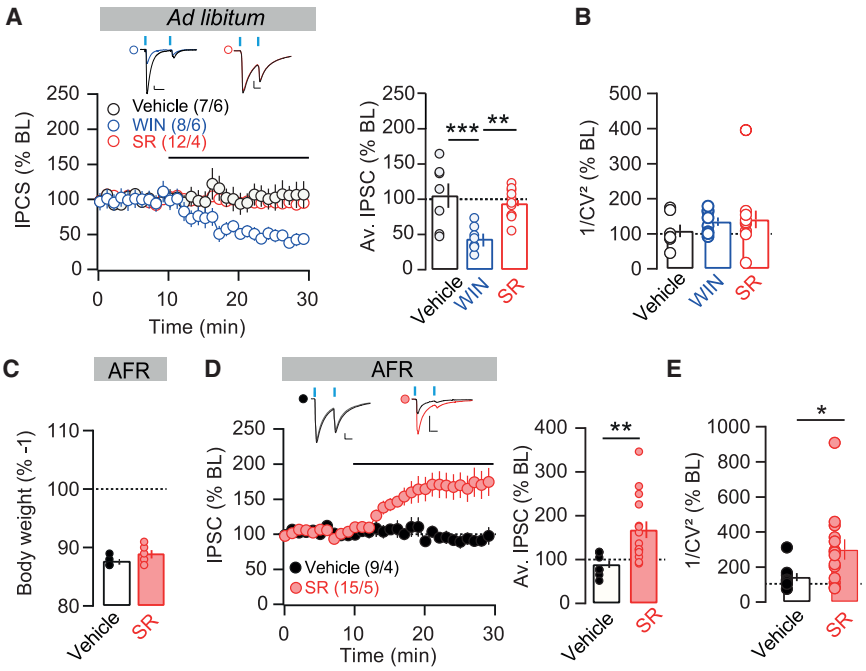

Figure 4. Transmission at D1-MSN-to-LH Synapses Is Modulated by CB1R Signaling

(A) Left: norm. IPSC for all cells with application WIN55,212-2 (2 μM), SR141617A (5 μM), or control recordings in slices of *ad libitum*-fed mice. Right: average IPSC (% BL) of the last 5 min of recording. CB1R agonist application significantly decreased IPSCs. ANOVA: $F(2,24) = 10.9$, $p < 0.01$; for vehicle versus WIN: $t(24) = 4.229$, $p < 0.001$; for WIN versus SR: $t(24) = 3.918$, $p < 0.01$.

(B) Coefficients of variation of the amplitude.

(C) D1Cre mice with floxed-ChR2 in NAcSh were food restricted overnight (AFR), and plasticity at D1-MSN-to-LH synapse was assessed the next day. Body weight (% day 1) was significantly reduced in AFR mice.

(D) Left: normalized IPSCs for SR141617A or vehicle applied to LH brain slices from AFR mice. Right: average norm. IPSCs of the last 5 min of recordings show significantly increased IPSCs after application of SR141716A. $t(22) = 3.050$, $p < 0.01$.

(E) $1/CV^2$ was significantly increased by SR141617A. $t21 = 2.113$, $^*p < 0.05$.

Bars represent means ± SEMs. $^*p < 0.05$, $^{**}p < 0.01$, $^{***}p < 0.001$.

in the NAcSh. Light-evoked IPSCs were monitored while recording from LH neurons and the CB1R agonist WIN55,212-2 was applied to the recording bath (Figures 4A and 4B). This orexigenic agonist induced a robust LTD of the D1-MSN-to-LH synapse (Figure 4A), which is consistent with our hypothesis that decreased synaptic transmission at the D1-MSN-to-LH synapse promotes increased feeding. Notably, applying the selective CB1R antagonist SR141716A in the same preparation did not change the amplitude of inhibitory postsynaptic currents at D1-MSN-to-LH synapses (Figure 4A). The coefficient of variation measures were not changed after WIN55,212 or SR141716A application (Figure 4B). If tonic CB1R activation is responsible for reduced synaptic transmission at D1-MSN-to-LH synapses after AFR, then blockade of this receptor in slices obtained from AFR mice should be sufficient to reveal plasticity. To test this hypothesis, we applied the CB1R antagonist SR141716A in LH slices of AFR mice while activating D1-MSN terminals (Figures 4C–4E). SR141716A application at cells recorded from AFR mice increased both the amplitudes and variances of the IPSCs (Figures 4D and 4E). Thus, direct blockade of CB1R in slices of AFR mice is sufficient to recapitulate the i-LTP induced by FSK, suggesting a pivotal role of tonic CB1R signaling in reducing inhibitory transmission at D1-MSN-to-LH synapses to drive overeating in food-restricted mice.

Overeating Is Modulated by Endocannabinoid Signaling at D1-MSN-to-LH Terminals

We further investigated whether AFR-induced plasticity could be blocked *in vivo* by systemic treatment with a CB1R antagonist, and ultimately aimed to causally link endocannabinoid effects at the D1-MSN-to LH synapse with food intake control. To this end, D1cre mice expressing ChR2 in the NAcSh underwent AFR and were injected with SR141716A (10 mg/kg, intraperitoneally [i.p.]) at the beginning of food restriction (~1800 h) and again the following morning, ~1 h before the electrophysiological recordings (Figure 5A). Control animals were either subjected to AFR and injected with vehicle or *ad libitum* fed and injected with SR141716A or vehicle. Body weight was significantly reduced following AFR in comparison to *ad libitum*-fed mice. Also SR141716A treatment decreased body weight, but equally in both groups (Figure 5B; ANOVA: feeding condition × treatment interaction, $F(1,28) = 0.036$, $p = 0.85$). As expected, in *ad libitum*-fed control mice injected with vehicle or SR141716A, application of FSK did not induce the potentiation of the D1-MSN-to-LH synapse (Figure 5C). Also consistent with the previous experiment, control AFR mice injected with vehicle showed robust FSK-induced i-LTP (Figure 5C). However, FSK failed to elicit i-LTP in AFR mice injected with SR141716A (Figure 5C; summary plot in Figure 5D). These data demonstrate that CB1R signaling during AFR is required for a weakening of the D1-MSN-to-LH synaptic inhibitory transmission.

Compensatory overeating occurs in response to acute food restriction in an effort to recover the caloric deficit. If the LTD at D1-MSN-to-LH synapses was involved in this overeating, then blocking the plasticity induction with SR141716A should also be sufficient to limit this behavioral response. To monitor overeating, wild-type *ad libitum*-fed mice were trained to lick a high-fat solution (Lipofundin, 5% v/v in water) once daily during a 1-h session. Using this approach, individual licks could be reliably monitored, allowing analysis of the feeding microstructure. A within-subject crossover 2 × 2 design was used in which mice were exposed to all 4 experimental conditions (AFR or *ad libitum* fed; vehicle or SR141716A injections) in a randomized order with at least 1 week of recovery between each test (Figures 5E–5H). As for the plasticity experiments, injections were given once at the start of AFR (~1800 h) and again the following morning, ~1 h before the lick test session. *Ad libitum*-fed animals received injections at the

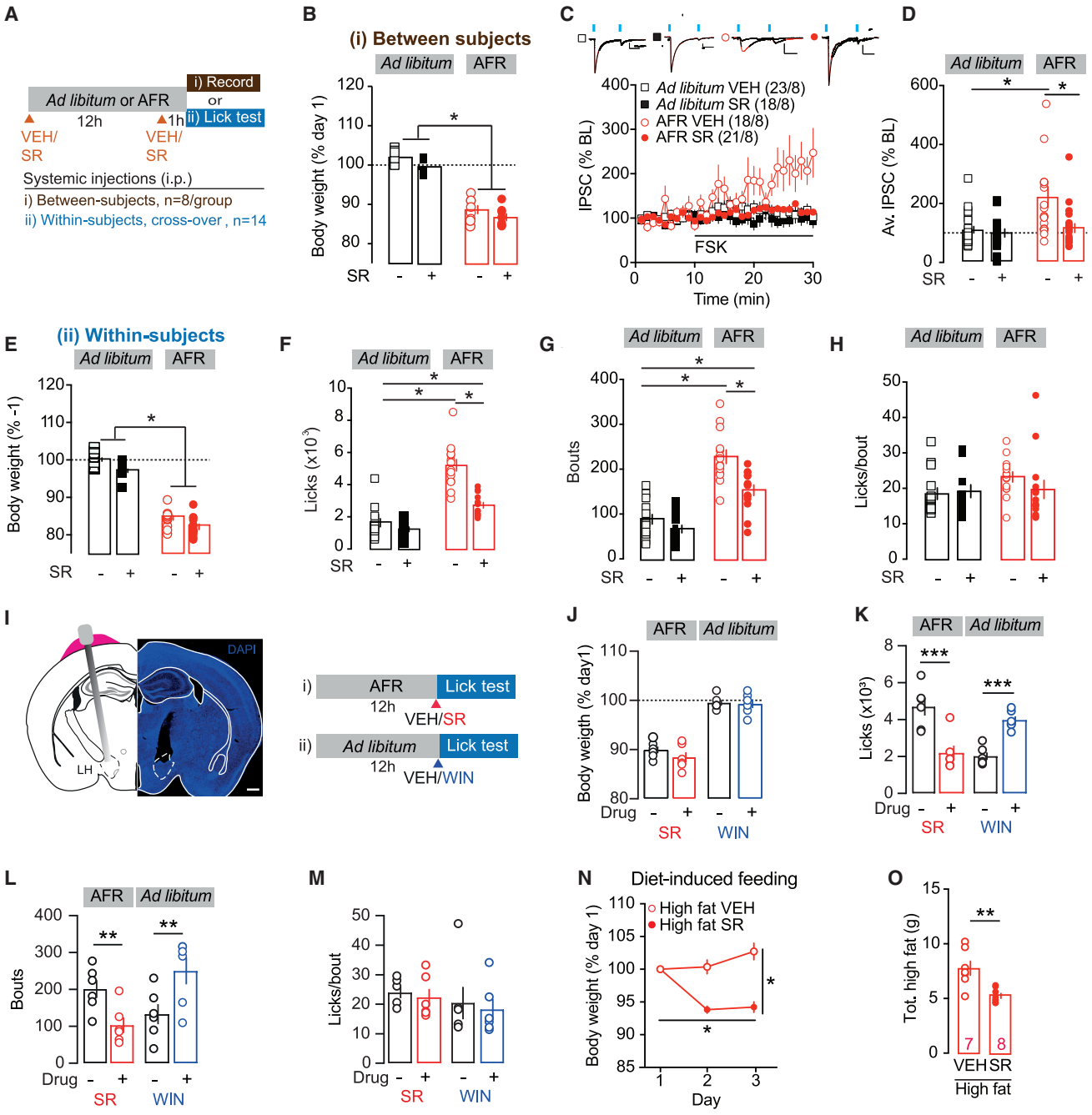

Figure 5. CB1R Signaling Is Required for D1-MSN-to-LH Plasticity after AFR and Concomitant Overeating

(A) Protocol for blockade of CB1R signaling with SR141716A in AFR or control groups. See Method Details for further details.

(B) Body weight (% day 1) was significantly decreased in AFR mice versus controls. ANOVA: feeding condition, $F(1,28) = 259.22$, $p < 0.01$. SR141716A treatment also significantly reduced body weight ANOVA: treatment, $F(1,28) = 6.75$, $p < 0.05$, but equally in both AFR and control mice. ANOVA: feeding condition × treatment interaction, not significant.

(C) Norm. IPSCs during bath application of FSK averaged for all cells and groups.

(D) Average IPSC (% BL) of the last 5 min of recording for all groups. FSK-induced i-LTP was present only in AFR mice injected with vehicle. This plasticity was prevented in AFR mice injected with SR141716A, and plasticity in these mice did not significantly differ from control VEH mice. ANOVA: feeding condition × treatment interaction, $F(1,76) = 5.09$, $p < 0.05$.

(E) Body weight (% day 1) was significantly decreased in AFR mice versus controls. ANOVA: effect of feeding condition, $F(1,13) = 629.95$, $p < 0.01$. Also, SR141716A treatment significantly reduced body weight. ANOVA: treatment, $F(1,13) = 34.97$, $p < 0.01$) but did so in both feeding conditions. ANOVA: feeding condition × treatment interaction, not significant.

(legend continued on next page)

same time points. AFR significantly reduced body weight as compared to when mice were fed *ab libitum*, and so did SR141716A treatment, but equally in both AFR and control mice (Figure 5E; ANOVA: feeding condition × treatment interaction, $F(1,13) = 0.29$, $p = 0.59$). Mice exposed to AFR and injected with vehicle showed a significant increase in the total number of licks in comparison to the *ad libitum*-fed test session (Figure 5F). This overeating was largely driven by a significant increase in bout number (Figure 5G), a measure reflecting motivational drive (Dwyer, 2012), while the number of licks per bout, considered a measure of palatability (Dwyer, 2012; Ellacott et al., 2010), remained unchanged (Figure 5H). Treatment with SR141716A during AFR significantly reduced this overeating response (Figures 5F–5H), suggesting that CB1R -signaling is required to induce compensatory overeating following acute food restriction.

To test the implication of CB1R directly in the LH, feeding was assessed after intra-LH infusions of the CB1R antagonist or CB1R agonist before testing the animals. In this experiment, mice were implanted bilaterally with cannulas targeting the LH and exposed to active compounds or vehicle in a randomized order with at least 1 week of recovery between each assessment (Figures 5I and 5J). Licking behavior was assessed just after the infusion. In AFR mice, intra-LH infusion of the CB1R antagonist decreased the number of licks and bouts. Conversely, mice fed *ad libitum* and infused with the CB1R agonist increased their consumption (Figures 5K and 5L). The number of licks per bout measure was not affected (Figure 4M).

Finally, we tested whether the blockade of CB1R signaling would prevent overeating driven by high-fat diets. Two groups of wild-type mice were fed a high-fat diet for 3 days and injected either with SR141716A (10 mg/kg, i.p.) or vehicle once every 12 h over the 3 days. Body weight (Figure 5N) and high fat consumption (Figure 5O) were monitored and significantly decreased in animals injected with SR141716A compared to vehicle controls.

These data show that CB1R signaling at the D1-MSN-to-LH connection plays a critical role in maintaining overeating in food-restricted mice, and the same mechanism may be engaged in mice fed with high-calorie and palatable foods.

D1-MSN-to-LH Plasticity Gates Overeating in Food-Restricted Animals

If i-LTP at the NAc D1-MSN-to-LH synapse is essential for overeating behavior, then artificially potentiating these synapses alone should be sufficient to decrease food consumption, even in hungry animals. To test this prediction, we selectively transfected D1-MSNs by injecting a floxed ChETA construct into the NAc of D1Cre mice and implanted optic fibers bilaterally targeting the LH (Figure 6A). Next, we tested the ability of a high-frequency stimulation protocol (HFS; ×4[100 pulses at 100 Hz, 20 s inter-stimulation interval (ISI)]), previously used to efficiently potentiate inhibitory synapses (Creed et al., 2016), to reduce consumption in food-restricted animals (Figures 6A and 6B). *In vivo* potentiation of the NAc D1-MSN-to-LH synapse significantly reduced the number of licks and bouts in food-restricted animals (Figures 6C–6E), mimicking our prior observation with LH infusions of the CB1R antagonist (Figures 5I–5M). The same HFS protocol failed to potentiate inhibitory transmission at D1-MSN-to-LH synapses in *ex vivo* brain slices from food-restricted animals (Figure S4A), except when the D1 agonist SFK38393 (10 μM) was present (Figures S4B–S4D). Akin to D1-MSN-to-VTA, the potentiation of inhibitory transmission requires the activation of presynaptic D1 receptors (Bocklisch et al., 2013). Our data suggest that endogenous dopamine signaling via D1 receptors in the LH is required *in vivo*, but it may be absent in the *ex vivo* slice preparation. These results clearly implicate synaptic plasticity specifically at the D1-MSN-to-LH synapse in gating overeating in fasted animals.

DISCUSSION

Here, we explored the contribution of synaptic plasticity to the regulation of adaptive feeding by the NAcSh-to-LH pathway,

(F) Total licks during 1-h lick test were significantly increased in AFR mice compared to control group, but SR141716A decreased total licks in AFR mice. ANOVA: feeding condition × treatment interaction, $F(1,13) = 44.63$, $p < 0.01$.

(G) Same as (F), but for number of bouts. Bout number was significantly increased in AFR mice injected with vehicle, and significantly decreased from this group in AFR mice injected with SR. ANOVA: feeding condition × treatment interaction: $F(1,13) = 8.83$, $p < 0.05$

(H) Total number of licks per bouts was not affected by AFR or the CB1R antagonist.

(I) Protocol for blockade of intra-LH infusion of CB1R antagonist in AFR mice and CB1R in *ad libitum*-fed mice. See Method Details for further details.

(J) Body weight.

(K) The number of licks was significantly decreased by SR in AFR mice. Oppositely, intra-LH WIN increased intake in mice fed *ad libitum*. ANOVA: feeding condition × treatment interaction: $F(1,10) = 75.61$, $p < 0.001$.

(L) The number of bouts was decreased by SR in AFR mice and increased by WIN in mice fed *ad libitum*. ANOVA: feeding condition × treatment interaction: $F(1,10) = 51.22$, $p < 0.001$.

(M) The number of licks per bout was not affected by feeding condition or treatments.

(N) C57BL/6J mice were fed a high-fat diet for 3 days and injected with SR141716A or vehicle once every 12 h. Body weight (% day 1) at day 3 was significantly decreased in mice injected with SR141716A as compared to vehicle. ANOVA: treatment × day interaction: $F(2,26) = 27.728$, $p < 0.01$; SR versus vehicle (VEH) group at day 3; unpaired t test, $t13 = -5.797$, $p < 0.01$; for SR141716A group day 3 versus day 1, paired t test, $t7 = 7.144$, $p < 0.01$; for VEH group day 3 versus day 1, body weight tended to increase, $t6 = -2.142$, $p = 0.076$.

(O) Total high-fat consumption (G) over the 3 treatment days was decreased in mice treated with SR141716A as compared to vehicle-injected mice. **Unpaired t test, $t13 = -3.90$, $p < 0.01$.

Representative traces show a mean of 30 sweeps during baseline (black) and at the end of recording (red), after HFS application.

Representative traces show a mean of 30 sweeps during baseline (black) and at the end of recording (red), after FSK application.

Bonferroni corrected t tests for 4 comparisons, *$p < 0.05$, **$p < 0.01$, ***$p < 0.001$.

Scale bars, 50 pA, 20 ms.

Plots show means ± SEMs.

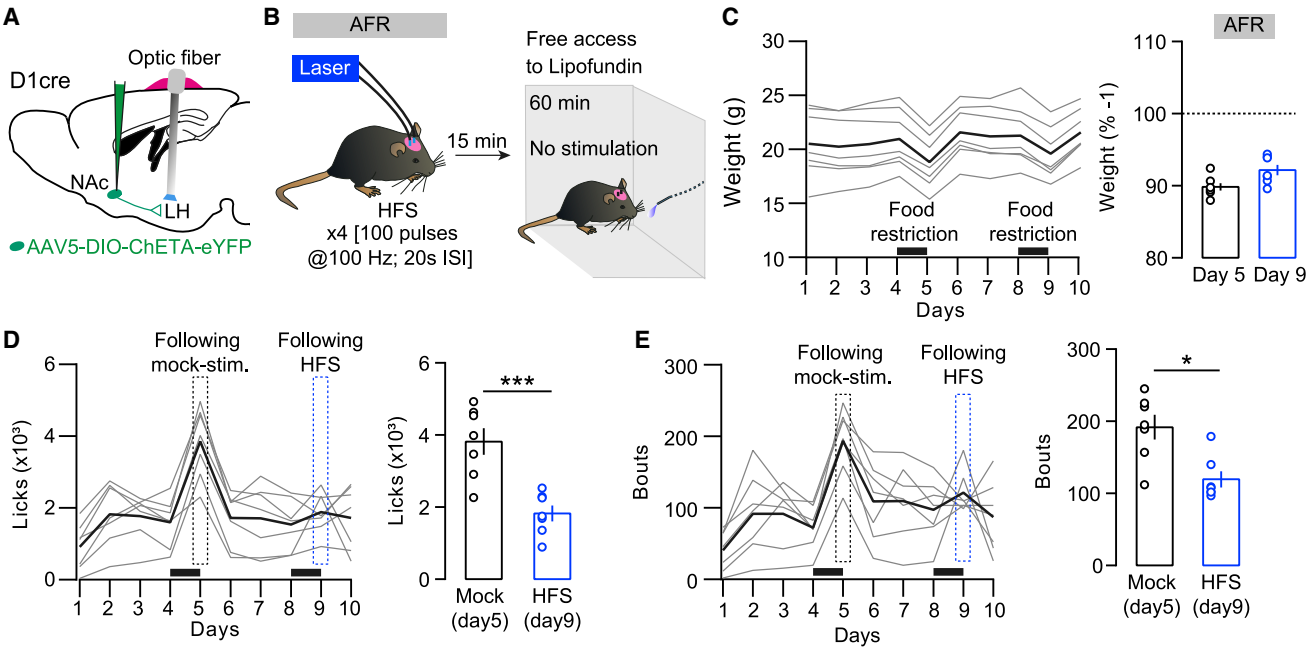

Figure 6. High-Frequency Stimulation at D1-MSN-to-LH Synapses Reduces Overeating in Food-Restricted Mice

(A) Surgical strategy to stimulate D1-MSN terminals in the LH *in vivo*.

(B) High-frequency stimulation protocol (HFS) and experiment timeline. Mice were stimulated 15 min before a 60-min session to assess food consumption (stimulation-free).

(C) Left: body weight in grams. Mice were food restricted 24 h before being tested for food intake. Black bars indicate the 24-h food restriction periods. Right: average body weight loss (%) after 24 h food restriction.

(D) Left: average licks per days. A mocked stimulation was performed 24 h after the first episode of food restriction. Dashed rectangles represent the results obtained 15 min after the stimulation protocols. Right: the number of licks was significantly decreased after HFS. $t6 = 6.534$, $p < 0.001$.

(E) Left: average bouts of consumption over days. Right: the number of bouts was also decreased in mice submitted to the HFS protocol. $t6 = 3.413$, $p < 0.05$.

In (C)–(E), bold lines represent the mean.

Bars represent means ± SEMs. *$p < 0.05$, ***$p < 0.001$.

which we previously found comprises mostly D1-MSNs (O'Connor et al., 2015). In *ad libitum*-fed animals, no potentiation of inhibitory synaptic transmission was elicited by established protocols effective at other major output targets of D1-MSNs (Bocklisch et al., 2013; Creed et al., 2016). This may reflect a unique property of NAcSh D1-MSN-to-LH projectors, as we showed that they are a largely distinct population from those projecting to the VP or VTA. The depressed transmission of D1-MSN-to-LH synapses was revealed by FSK potentiation under states favoring overeating, either following acute food restriction or when mice were provided solely with high-fat diets. In slices from mice fed regular lab chow, the D1-MSN-to-LH synapse underwent robust i-LTD upon CB1R activation. CB1R blockade during AFR prevented both the FSK-induced i-LTP that normally developed in this condition and subsequent overeating driven by AFR or high-fat diets. Lateral hypothalamic infusions of CB1R agonists and antagonists also induced or prevented overeating, respectively. Finally, *in vivo* HFS specifically at the D1-MSN-to-LH synapse reduced consumption in food-restricted animals. Our data suggest that endocannabinoid signaling induces depression at the NAcSh-to-LH circuit to gate overeating.

In our study, the NAcSh-to-LH pathway emerges as anatomically and functionally distinct from other major output projections of accumbens. A recent study found that D1-MSNs projections to the VP and VTA largely overlap (Pardo-Garcia et al., 2019) and exhibit shared mechanisms of synaptic plasticity (Bocklisch et al., 2013; Creed et al., 2016). Here, D1-MSN-to-LH projectors rarely overlapped with NAcSh-to-VP or -VTA projectors, despite soma being intermingled. That being said, clustering of NAcSh-to-VP projection soma was seen in the most rostral aspect of NAcSh, while the few putative D2-MSN-to-LH projections were most often found caudally. Such rostro-caudal anatomical gradients may explain in part corresponding functional gradients ascribed to accumbens elsewhere (Castro and Berridge, 2014). Different projection populations may hold distinct gene expression profiles and divergent input architecture and be subject to unique synaptic environments in the target nucleus; any of these factors may contribute to the distinct basal synaptic properties seen in the D1-MSN-to-LH pathway. With respect to the function of plasticity, potentiation of the NAcSh-to-VP and -VTA synapses have been implicated in drug-adaptive behaviors, including locomotor sensitization to cocaine (Bocklisch et al., 2013; Creed et al., 2016; Melis et al., 2002; Nugent et al., 2007), while here, we establish a critical role for inhibitory synaptic plasticity in the NAcSh-to-LH pathway in feeding control. Further study will be required to know how plasticity mechanisms in this pathway support

other motivated behaviors, including drug-adaptive behaviors relevant to addiction (Gibson et al., 2018).

In addition to LH VGAT neurons (O'Connor et al., 2015), here, we identify a second population of LH neurons receiving D1-MSN inhibition and expressing VGluT2. This is perhaps surprising given the opposite roles ascribed to LH VGAT and VGluT2 neurons in feeding (Jennings et al., 2013, 2015; O'Connor et al., 2015; Stamatakis et al., 2016). However, a recent transcriptomic analysis identified up to 30 distinct subpopulations of LH GABA and glutamate neurons that differ in their gene expression profiles (Mickelsen et al., 2019). There are also clear differences in LH neuron function when the projection target is considered. For instance, LH GABA neuron projections to the VTA are associated with diverse functions, including feeding, positive reinforcement, social interaction, and object exploration (Nieh et al., 2015, 2016). In contrast, LH GABA neurons projecting to the periaqueductal gray matter (PAG) mediate predatory behavior (Li et al., 2018), while the activation of LH GABA projections to the paraventricular hypothalamus increased consumption (Wu et al., 2015). LH glutamate neurons have been found to project to the VTA (de Jong et al., 2018; Nieh et al., 2016) and lateral habenula (Lazaridis et al., 2019; Lecca et al., 2017; Stamatakis et al., 2016) and contribute to the processing and generation of adaptive responses to aversive stimuli. While our observation shows that food restriction affects LH GABA and glutamatergic neurons similarly, an important avenue for future research will be to fully resolve the input-output connectivity map of different LH neuron populations to better understand the function of this complex nucleus.

The role of endocannabinoids in regulating food intake is well described (Di Marzo et al., 2009). For example, CB1R agonists increase food intake (Williams and Kirkham, 2002), while CB1R antagonists are anorexigenic and have shown promise for the treatment of obesity (Di Marzo et al., 2009; Koch, 2017; Ravinet Trillou et al., 2003; Christensen et al., 2007). Fasting leads to increased levels of endocannabinoids in the nucleus accumbens and hypothalamic area (Kirkham et al., 2002), while fasting-induced overeating is decreased in CB1R-knockout (KO) mice as compared to wild-type controls (Di Marzo et al., 2001; Poncelet et al., 2003). Besides the general idea that activation of the endocannabinoid system increases food intake, evidence suggests there are other concomitant mechanisms through which this system is implicated in modulating synaptic transmission to regulate food intake. For instance, a study reported that food deprivation induced a glucocorticoid-mediated loss of CB1Rs at GABAergic synapses in the dorsomedial hypothalamus, a region known for signaling satiety. This loss led to an activity-dependent potentiation of GABAergic transmission in food-deprived animals, probably resulting in enhanced inhibition onto dorsomedial hypothalamic cells mediating satiety signals (Crosby et al., 2011).

Our data provide insight to suggest that CB1R signaling during fasting may serve to weaken synaptic strength at the D1-MSN-to-LH pathway, which then serves as a permissive signal to promote overeating when food again becomes available. Robust i-LTD could be elicited at this pathway when the CB1R agonist WIN-55,212-2 is applied directly onto LH slice preparation from *ad libitum*-fed animals. Conversely, i-LTP was revealed when applying the CB1R antagonist SR141716A onto *ex vivo* LH slices from AFR mice. By delivering CB1R antagonists and agonists directly to the LH, we could establish the sufficiency and necessity of CB1R signaling in this region to promote and prevent overeating, respectively. However, the use of both systemic injections and local infusion does not allow the ascertainment of the exact cellular location of the receptors involved. The cellular source of endocannabinoids also remains to be determined, but it is unlikely to be a direct consequence of inhibitory transmission as both anandamide and 2-arachidonoylglycerol (2-AG) are released in a Ca^{2+}-dependent manner upon the depolarization of neurons capable of synthesizing endocannabinoids (Wilson and Nicoll, 2001). From our data, however, it is tempting to speculate that the necessary CB1Rs are located on D1R-MSN terminals in LH.

Three days of high-fat diet exposure has been linked with increased levels of endocannabinoids in the hypothalamus (Higuchi et al., 2011), which we speculate may also drive the plasticity of the D1-MSN-to-LH synapse via CB1Rs to support overeating of a calorically dense diet. Important questions remain: would this plasticity persist with chronic exposure to a high-fat diet? What would be the temporal dynamics of its recovery when the high-fat diet is withdrawn? How might this plasticity contribute to continued overeating eventually leading to obesity?

In modern society, with highly palatable and calorically dense foods readily available, chronic hypoactivity of the NAcSh-to-LH pathway may represent a point of susceptibility to engender persistent overeating leading to weight gain and obesity. Our findings warrant further inspection of this pathway in the context of eating disorders and may inspire novel targeted approaches as a means to recover the synaptic strength of the NAcSh-to-LH pathway to ultimately regain control over compulsive overeating.

STAR★METHODS

Detailed methods are provided in the online version of this paper and include the following:

- KEY RESOURCES TABLE
- RESOURCE AVAILABILITY
  - Lead Contact
  - Materials Availability
  - Data and Code Availability
- EXPERIMENTAL MODEL AND SUBJECT DETAILS
  - Animals
- METHOD DETAILS
  - Surgery
  - Channelrhodopsin injections
  - Infusion cannulas implantation
  - Optic fiber implantation
  - Neuronal tracing with CTB
  - Monosynaptic rabies tracing
  - Whole-cell electrophysiology
  - *In vivo* experiments
  - Acute food restriction (AFR)
  - Plasticity after 7 days from AFR
  - Systemic delivery of CB1R antagonist
  - Local infusion of CB1R antagonist/agonist
  - Optogenetic HFS experiments

SUPPLEMENTAL INFORMATION

Supplemental Information can be found online at https://doi.org/10.1016/j.neuron.2020.03.029.

ACKNOWLEDGMENTS

This work was financed by the Swiss National Science Foundation (CRSII5_183524) and by an advanced grant from the European Research Council (MeSSI). We thank all of the members of the Lüscher laboratory for their discussion and feedback on the manuscript. We thank S. LeFort for assistance with *ex vivo* electrophysiology recordings made in VGluT2cre mice. We thank Masaya Harada for the assistance in behavioral manipulation before the patch clamp experiments (body weight measures, food deprivation). We thank C. Gerfen for providing D1Cre-mouse lines through the Mutant Mouse Resource and Research Center (MMRRC) repository.

AUTHOR CONTRIBUTIONS

S.T., E.C.O., M.L., and C.L. conceived the experiments. S.T. executed the electrophysiology for plasticity studies and the behavioral experiments. M.L. performed the electrophysiology and behavioral experiments. E.C.O. performed the electrophysiology for connectivity studies and the neural tracing. All of the authors contributed to writing the manuscript.

DECLARATION OF INTERESTS

C.L. is a member of the scientific advisory boards of the International Foundation for Research in Paraplegia and the Phenix Foundation. E.C.O. is currently a full-time employee of F. Hoffmann-La Roche AG.

Received: April 19, 2019
Revised: February 21, 2020
Accepted: March 25, 2020
Published: April 24, 2020

REFERENCES

Arrigoni, E., Chee, M.J.S., and Fuller, P.M. (2019). To eat or to sleep: that is a lateral hypothalamic question. Neuropharmacology *154*, 34–49.

Atwood, B.K., Lovinger, D.M., and Mathur, B.N. (2014a). Presynaptic long-term depression mediated by Gi/o-coupled receptors. Trends Neurosci. *37*, 663–673.

Atwood, B.K., Kupferschmidt, D.A., and Lovinger, D.M. (2014b). Opioids induce dissociable forms of long-term depression of excitatory inputs to the dorsal striatum. Nat. Neurosci. *17*, 540–548.

Berridge, K.C. (2009). 'Liking' and 'wanting' food rewards: brain substrates and roles in eating disorders. Physiol. Behav. *97*, 537–550.

Bocklisch, C., Pascoli, V., Wong, J.C.Y., House, D.R.C., Yvon, C., de Roo, M., Tan, K.R., and Lüscher, C. (2013). Cocaine disinhibits dopamine neurons by potentiation of GABA transmission in the ventral tegmental area. Science *341*, 1521–1525.

Bonnavion, P., Mickelsen, L.E., Fujita, A., de Lecea, L., and Jackson, A.C. (2016). Hubs and spokes of the lateral hypothalamus: cell types, circuits and behaviour. J. Physiol. *594*, 6443–6462.

Brown, M.T., Tan, K.R., O'Connor, E.C., Nikonenko, I., Muller, D., and Lüscher, C. (2012). Ventral tegmental area GABA projections pause accumbal cholinergic interneurons to enhance associative learning. Nature *492*, 452–456.

Burnett, C.J., Li, C., Webber, E., Tsaousidou, E., Xue, S.Y., Brüning, J.C., and Krashes, M.J. (2016). Hunger-Driven Motivational State Competition. Neuron *92*, 187–201.

Castillo, P.E., Chiu, C.Q., and Carroll, R.C. (2011). Long-term plasticity at inhibitory synapses. Curr. Opin. Neurobiol. *21*, 328–338.

Castro, D.C., and Berridge, K.C. (2014). Opioid hedonic hotspot in nucleus accumbens shell: mu, delta, and kappa maps for enhancement of sweetness "liking" and "wanting". J. Neurosci. *34*, 4239–4250.

Christensen, R., Kristensen, P.K., Bartels, E.M., Bliddal, H., and Astrup, A. (2007). Efficacy and safety of the weight-loss drug rimonabant: a meta-analysis of randomised trials. Lancet *370*, 1706–1713.

Cortés-Salazar, F., Suárez Ortíz, J.O., Cendejas Trejo, N.M., Mancilla-Díaz, J.M., López-Alonso, V.E., and Escartín-Pérez, R.E. (2014). Efectos de la activación del receptor cannabinoide cb1 en el núcleo accumbens shell sobre la conducta alimentaria. Acta Colomb. Psicol. *17*, 61–68.

Creed, M., Ntamati, N.R., Chandra, R., Lobo, M.K., and Lüscher, C. (2016). Convergence of Reinforcing and Anhedonic Cocaine Effects in the Ventral Pallidum. Neuron *92*, 214–226.

Crosby, K.M., Inoue, W., Pittman, Q.J., and Bains, J.S. (2011). Endocannabinoids gate state-dependent plasticity of synaptic inhibition in feeding circuits. Neuron *71*, 529–541.

de Jong, J.W., Afjei, S.A., Pollak Dorocic, I., Peck, J.R., Liu, C., Kim, C.K., et al. (2018). A Neural Circuit Mechanism for Encoding Aversive Stimuli in the Mesolimbic Dopamine System. Neuron *101*, 133–151.e7.

Di Marzo, V., Goparaju, S.K., Wang, L., Liu, J., Bátkai, S., Járai, Z., Fezza, F., Miura, G.I., Palmiter, R.D., Sugiura, T., and Kunos, G. (2001). Leptin-regulated endocannabinoids are involved in maintaining food intake. Nature *410*, 822–825.

Di Marzo, V., Ligresti, A., and Cristino, L. (2009). The endocannabinoid system as a link between homoeostatic and hedonic pathways involved in energy balance regulation. Int. J. Obes. *33* (*Suppl 2*), S18–S24.

Dwyer, D.M. (2012). EPS Prize Lecture. Licking and liking: the assessment of hedonic responses in rodents. Q. J. Exp. Psychol. (Hove) *65*, 371–394.

Ellacott, K.L.J., Morton, G.J., Woods, S.C., Tso, P., and Schwartz, M.W. (2010). Assessment of feeding behavior in laboratory mice. Cell Metab. *12*, 10–17.

Ferrario, C.R., Labouèbe, G., Liu, S., Nieh, E.H., Routh, V.H., Xu, S., and O'Connor, E.C. (2016). Homeostasis Meets Motivation in the Battle to Control Food Intake. J. Neurosci. *36*, 11469–11481.

Gibson, G.D., Prasad, A.A., Jean-Richard-Dit-Bressel, P., Yau, J.O.Y., Millan, E.Z., Liu, Y., Campbell, E.J., Lim, J., Marchant, N.J., Power, J.M., et al. (2018). Distinct Accumbens Shell Output Pathways Promote versus Prevent Relapse to Alcohol Seeking. Neuron *98*, 512–520.e6.

Hall, K.D., and Kahan, S. (2018). Maintenance of Lost Weight and Long-Term Management of Obesity. Med. Clin. North Am. *102*, 183–197.

Hambly, C., and Speakman, J.R. (2015). Mice that gorged during dietary restriction increased foraging related behaviors and differed in their macronutrient preference when released from restriction. PeerJ *3*, e1091.

Higuchi, S., Ohji, M., Araki, M., Furuta, R., Katsuki, M., Yamaguchi, R., Akitake, Y., Matsuyama, K., Irie, K., Mishima, K., et al. (2011). Increment of hypothalamic 2-arachidonoylglycerol induces the preference for a high-fat diet via activation of cannabinoid 1 receptors. Behav. Brain Res. *216*, 477–480.

Hu, S.S.J., Liu, Y.W., and Yu, L. (2015). Medial prefrontal cannabinoid CB1 receptors modulate consolidation and extinction of cocaine-associated memory in mice. Psychopharmacology (Berl.) *232*, 1803–1815.

Inoue, W., Baimoukhametova, D.V., Füzesi, T., Wamsteeker Cusulin, J.I., Koblinger, K., Whelan, P.J., Pittman, Q.J., and Bains, J.S. (2013). Noradrenaline is a stress-associated metaplastic signal at GABA synapses. Nat. Neurosci. *16*, 605–612.

Jennings, J.H., Rizzi, G., Stamatakis, A.M., Ung, R.L., and Stuber, G.D. (2013). The inhibitory circuit architecture of the lateral hypothalamus orchestrates feeding. Science *341*, 1517–1521.

Jennings, J.H., Ung, R.L., Resendez, S.L., Stamatakis, A.M., Taylor, J.G., Huang, J., Veleta, K., Kantak, P.A., Aita, M., Shilling-Scrivo, K., et al. (2015). Visualizing hypothalamic network dynamics for appetitive and consummatory behaviors. Cell *160*, 516–527.

Kirkham, T.C., Williams, C.M., Fezza, F., and Di Marzo, V. (2002). Endocannabinoid levels in rat limbic forebrain and hypothalamus in relation to fasting, feeding and satiation: stimulation of eating by 2-arachidonoyl glycerol. Br. J. Pharmacol. *136*, 550–557.

Koch, M. (2017). Cannabinoid receptor signaling in central regulation of feeding behavior: a mini-review. Front. Neurosci. *11*, 293.

Krause, M., German, P.W., Taha, S.A., and Fields, H.L. (2010). A pause in nucleus accumbens neuron firing is required to initiate and maintain feeding. J. Neurosci. *30*, 4746–4756.

Kupchik, Y.M., Brown, R.M., Heinsbroek, J.A., Lobo, M.K., Schwartz, D.J., and Kalivas, P.W. (2015). Coding the direct/indirect pathways by D1 and D2 receptors is not valid for accumbens projections. Nat. Neurosci. *18*, 1230–1232.

Lazaridis, I., Tzortzi, O., Weglage, M., Märtin, A., Xuan, Y., Parent, M., Johansson, Y., Fuzik, J., Fürth, D., Fenno, L.E., et al. (2019). A hypothalamus-habenula circuit controls aversion. Mol. Psychiatry *24*, 1351–1368.

Lecca, S., Meye, F.J., Trusel, M., Tchenio, A., Harris, J., Schwarz, M.K., Burdakov, D., Georges, F., and Mameli, M. (2017). Aversive stimuli drive hypothalamus-to-habenula excitation to promote escape behavior. eLife *6*, 1–16.

Li, Y., Zeng, J., Zhang, J., Yue, C., Zhong, W., Liu, Z., Feng, Q., and Luo, M. (2018). Hypothalamic Circuits for Predation and Evasion. Neuron *97*, 911–924.e5.

Maldonado-Irizarry, C.S., Swanson, C.J., and Kelley, A.E. (1995). Glutamate receptors in the nucleus accumbens shell control feeding behavior via the lateral hypothalamus. J. Neurosci. *15*, 6779–6788.

Martín, A.B., Fernandez-Espejo, E., Ferrer, B., Gorriti, M.A., Bilbao, A., Navarro, M., Rodriguez de Fonseca, F., and Moratalla, R. (2008). Expression and function of CB1 receptor in the rat striatum: localization and effects on D1 and D2 dopamine receptor-mediated motor behaviors. Neuropsychopharmacology *33*, 1667–1679.

Mebel, D.M., Wong, J.C.Y., Dong, Y.J., and Borgland, S.L. (2012). Insulin in the ventral tegmental area reduces hedonic feeding and suppresses dopamine concentration via increased reuptake. Eur. J. Neurosci. *36*, 2336–2346.

Melis, M., Camarini, R., Ungless, M.A., and Bonci, A. (2002). Long-lasting potentiation of GABAergic synapses in dopamine neurons after a single in vivo ethanol exposure. J. Neurosci. *22*, 2074–2082.

Mickelsen, L.E., Bolisetty, M., Chimileski, B.R., Fujita, A., Beltrami, E.J., Costanzo, J.T., Naparstek, J.R., Robson, P., and Jackson, A.C. (2019). Single-cell transcriptomic analysis of the lateral hypothalamic area reveals molecularly distinct populations of inhibitory and excitatory neurons. Nat. Neurosci. *22*, 642–656.

Morris, M.J., Beilharz, J.E., Maniam, J., Reichelt, A.C., and Westbrook, R.F. (2015). Why is obesity such a problem in the 21st century? The intersection of palatable food, cues and reward pathways, stress, and cognition. Neurosci. Biobehav. Rev. *58*, 36–45.

Morton, G.J., Meek, T.H., and Schwartz, M.W. (2014). Neurobiology of food intake in health and disease. Nat. Rev. Neurosci. *15*, 367–378.

Nieh, E.H., Matthews, G.A., Allsop, S.A., Presbrey, K.N., Leppla, C.A., Wichmann, R., Neve, R., Wildes, C.P., and Tye, K.M. (2015). Decoding neural circuits that control compulsive sucrose seeking. Cell *160*, 528–541.

Nieh, E.H., Vander Weele, C.M., Matthews, G.A., Presbrey, K.N., Wichmann, R., Leppla, C.A., Izadmehr, E.M., and Tye, K.M. (2016). Inhibitory Input from the Lateral Hypothalamus to the Ventral Tegmental Area Disinhibits Dopamine Neurons and Promotes Behavioral Activation. Neuron *90*, 1286–1298.

Nugent, F.S., Penick, E.C., and Kauer, J.A. (2007). Opioids block long-term potentiation of inhibitory synapses. Nature *446*, 1086–1090.

O'Connor, E.C., Kremer, Y., Lefort, S., Harada, M., Pascoli, V., Rohner, C., and Lüscher, C. (2015). Accumbal D1R Neurons Projecting to Lateral Hypothalamus Authorize Feeding. Neuron *88*, 553–564.

O'Connor, K.L., Scisco, J.L., Smith, T.J., Young, A.J., Montain, S.J., Price, L.L., Lieberman, H.R., and Karl, J.P. (2016). Altered Appetite-Mediating Hormone Concentrations Precede Compensatory Overeating After Severe, Short-Term Energy Deprivation in Healthy Adults. J. Nutr. *146*, 209–217.

Pardo-Garcia, T.R., Garcia-Keller, C., Penaloza, T., Richie, C.T., Pickel, J., Hope, B.T., Harvey, B.K., Kalivas, P.W., and Heinsbroek, J.A. (2019). Ventral pallidum is the primary target for accumbens D1 projections driving cocaine seeking. J. Neurosci. *39*, 2041–2051.

Peciña, S., and Berridge, K.C. (2005). Hedonic hot spot in nucleus accumbens shell: where do mu-opioids cause increased hedonic impact of sweetness? J. Neurosci. *25*, 11777–11786.

Penicaud, L., and Le Magnen, J. (1980). Recovery of body weight following starvation or food restriction in rats. Neurosci. Biobehav. Rev. *4* (*Suppl 1*), 47–52.

Pertwee, R.G. (2006). The pharmacology of cannabinoid receptors and their ligands: an overview. Int. J. Obes. *30* (*Suppl 1*), S13–S18.

Petrovich, G.D. (2018). Lateral Hypothalamus as a Motivation-Cognition Interface in the Control of Feeding Behavior. Front. Syst. Neurosci. *12*, 14.

Poncelet, M., Maruani, J., Calassi, R., and Soubrié, P. (2003). Overeating, alcohol and sucrose consumption decrease in CB1 receptor deleted mice. Neurosci. Lett. *343*, 216–218.

Ravinet Trillou, C., Arnone, M., Delgorge, C., Gonalons, N., Keane, P., Maffrand, J.-P., and Soubrié, P. (2003). Anti-obesity effect of SR141716, a CB1 receptor antagonist, in diet-induced obese mice. Am. J. Physiol. Regul. Integr. Comp. Physiol. *284*, R345–R353.

Rosenbaum, M., Kissileff, H.R., Mayer, L.E.S., Hirsch, J., and Leibel, R.L. (2010). Energy intake in weight-reduced humans. Brain Res. *1350*, 95–102.

Sohn, J.W., Elmquist, J.K., and Williams, K.W. (2013). Neuronal circuits that regulate feeding behavior and metabolism. Trends Neurosci. *36*, 504–512.

Soria-Gómez, E., Matias, I., Rueda-Orozco, P.E., Cisneros, M., Petrosino, S., Navarro, L., Di Marzo, V., and Prospéro-García, O. (2007). Pharmacological enhancement of the endocannabinoid system in the nucleus accumbens shell stimulates food intake and increases c-Fos expression in the hypothalamus. Br. J. Pharmacol. *151*, 1109–1116.

Sparta, D.R., Stamatakis, A.M., Phillips, J.L., Hovelsø, N., van Zessen, R., and Stuber, G.D. (2011). Construction of implantable optical fibers for long-term optogenetic manipulation of neural circuits. Nat. Protoc. *7*, 12–23.

Stamatakis, A.M., Jennings, J.H., Ung, R.L., Blair, G.A., Weinberg, R.J., Neve, R.L., Boyce, F., Mattis, J., Ramakrishnan, C., Deisseroth, K., and Stuber, G.D. (2013). A unique population of ventral tegmental area neurons inhibits the lateral habenula to promote reward. Neuron *80*, 1039–1053.

Stamatakis, A.M., Van Swieten, M., Basiri, M.L., Blair, G.A., Kantak, P., and Stuber, G.D. (2016). Lateral Hypothalamic Area Glutamatergic Neurons and Their Projections to the Lateral Habenula Regulate Feeding and Reward. J. Neurosci. *36*, 302–311.

Stratford, T.R., and Kelley, A.E. (1999). Evidence of a functional relationship between the nucleus accumbens shell and lateral hypothalamus subserving the control of feeding behavior. J. Neurosci. *19*, 11040–11048.

Stuber, G.D., and Wise, R.A. (2016). Lateral hypothalamic circuits for feeding and reward. Nat. Neurosci. *19*, 198–205.

Tandon, S., Keefe, K.A., and Taha, S.A. (2017). Mu opioid receptor signaling in the nucleus accumbens shell increases responsiveness of satiety-modulated lateral hypothalamus neurons. Eur. J. Neurosci. *45*, 1418–1430.

Urstadt, K.R., Kally, P., Zaidi, S.F., and Stanley, B.G. (2013). Ipsilateral feeding-specific circuits between the nucleus accumbens shell and the lateral hypothalamus: regulation by glutamate and GABA receptor subtypes. Neuropharmacology *67*, 176–182.

Varela, L., and Horvath, T.L. (2012). Leptin and insulin pathways in POMC and AgRP neurons that modulate energy balance and glucose homeostasis. EMBO Rep. *13*, 1079–1086.

Wamsteeker Cusulin, J.I., Füzesi, T., Inoue, W., and Bains, J.S. (2013). Glucocorticoid feedback uncovers retrograde opioid signaling at hypothalamic synapses. Nat. Neurosci. *16*, 596–604.

Watabe-Uchida, M., Zhu, L., Ogawa, S.K., Vamanrao, A., and Uchida, N. (2012). Whole-brain mapping of direct inputs to midbrain dopamine neurons. Neuron *74*, 858–873.

Waterson, M.J., and Horvath, T.L. (2015). Neuronal Regulation of Energy Homeostasis: Beyond the Hypothalamus and Feeding. Cell Metab. *22*, 962–970.

Wei, N., Wang, Y., Wang, X., He, Z., Zhang, M., Zhang, X., Pan, Y., Zhang, J., Qin, Z., and Zhang, K. (2015). The different effects of high-frequency stimulation of the nucleus accumbens shell and core on food consumption are possibly associated with different neural responses in the lateral hypothalamic area. Neuroscience *301*, 312–322.

Will, M.J., Franzblau, E.B., and Kelley, A.E. (2003). Nucleus accumbens mu-opioids regulate intake of a high-fat diet via activation of a distributed brain network. J. Neurosci. *23*, 2882–2888.

Williams, C.M., and Kirkham, T.C. (2002). Observational analysis of feeding induced by Delta9-THC and anandamide. Physiol. Behav. *76*, 241–250.

Wilson, R.I., and Nicoll, R.A. (2001). Endogenous cannabinoids mediate retrograde signalling at hippocampal synapses. Nature *410*, 588–592.

Wu, Z., Kim, E.R., Sun, H., Xu, Y., Mangieri, L.R., Li, D.-P., Pan, H.L., Xu, Y., Arenkiel, B.R., and Tong, Q. (2015). GABAergic projections from lateral hypothalamus to paraventricular hypothalamic nucleus promote feeding. J. Neurosci. *35*, 3312–3318.

Yang, H., de Jong, J.W., Tak, Y., Peck, J., Bateup, H.S., and Lammel, S. (2018). Nucleus Accumbens Subnuclei Regulate Motivated Behavior via Direct Inhibition and Disinhibition of VTA Dopamine Subpopulations. Neuron *97*, 434–449.e4.

Zhang, M., and Kelley, A.E. (2000). Enhanced intake of high-fat food following striatal mu-opioid stimulation: microinjection mapping and fos expression. Neuroscience *99*, 267–277.

STAR★METHODS

KEY RESOURCES TABLE

REAGENT or RESOURCE	SOURCE	IDENTIFIER
Chemicals, Peptides, and Recombinant Proteins		
Cholera-toxin subunit B	Thermo Fisher Scientific, Massachussetts, USA	Cat. No. C22841
DAPI	Abcam, Cambridge, UK	RRID: AB_104139
Foskolin	Tocris Biosciences, Bristol, UK	Cat. No. 1099
WIN 55,212-2 mesylate	Tocris Biosciences, Bristol, UK	Cat. No. 1038
DAMGO	Tocris Biosciences, Bristol, UK	Cat. No. 1171
SR 141716A	Tocris Biosciences, Bristol, UK	Cat. No. 0923
SKF 38393 hydrobromide	Tocris Biosciences, Bristol, UK	Cat. No. 0922
Dimethyl Sulfoxide (DMSO)	Sigma-Aldrich, Missouri, USA	Cat. No. D2650
Experimental Models: Organisms/Strains		
D1Cre mice (B6;129-Tg(Drd1-cre)120Mxu/Mmjax)	The Jackson Laboratories, Main, USA	Stock No: 37156
VGATCre mice (Slc32a1 < tm2(cre)Lowl)	The Jackson Laboratories, Main, USA	Stock No: 016962
VGluT2Cre mice (Slc17a6 < tm2(cre)Lowl)	The Jackson Laboratories, Main, USA	Stock No: 016963
D1rd1a-tdTomato mice (B6.Cg-Tg(Drd1a-tdTomato) 6Calak/J)	The Jackson Laboratories, Main, USA	Stock No: 016204
Bacterial and Virus Strains		
AAV5-EF1A-DIO-ChR2(H134R)-eYFP	UNC Vector Core, North Carolina, USA	N/A
AAV5-EF1A-DIO-ChETA-EYFP	UNC Vector Core, North Carolina, USA	N/A
AAV5-DIO-EF1A-mCherry	UNC Vector Core, North Carolina, USA	N/A
AAV5-hsyn-ChR2(H134R)-eYFP	UNC Vector Core, North Carolina, USA	N/A
AAV5-DIO-EF1A-tdTomato	UNC Vector Core, North Carolina, USA	N/A
AAV5-Flex-TVA-mCherry	UNC Vector Core, North Carolina, USA	N/A
AAV8-Flex-RG	UNC Vector Core, North Carolina, USA	N/A
SADΔG-EFG(EnvA)	Salk Institute Vector Core, California, USA	32635 (Addgene)
Other		
Mouse Diet, High Fat, Fat Calories (60%)	Bio-Serv, New Jersey, USA	Product No: F3282

RESOURCE AVAILABILITY

Lead Contact

Further information and resources and reagents are availble on 10.5281/zenodo.3712745 or directly from the Lead Contact, Christian Lüscher (Christian.Luscher@unige.ch).

Materials Availability

This study did not generate new unique reagents.

Data and Code Availability

The published article includes all datasets generated or analyzed during this study. Original data have been deposited to Zenodo (accession number above).

EXPERIMENTAL MODEL AND SUBJECT DETAILS

Animals

All experiments were performed in accordance with the Institutional Animal Care and Use Committee of the University of Geneva and the Cantonal Authorities. Male and female mice were subjected to experimental procedures when at least 3 weeks old with littermates of both sexes randomly allocated to experimental groups. The genotype and number of mice used for each experiment is summarized in Tables S1–S3.

Animals were maintained on a 12:12h light-dark cycle (lights on at 7:00) in a temperature (21 ± 2°C) and humidity (50 ± 5%) controlled environment. Except when otherwise detailed, water and chow (Product code, 801067; Special Diets Services, Witham, UK) were available *ad libitum*. Experiments were performed during the light cycle. Single-housing was necessary for experiments requiring exact measures of food intake or food restriction and it is explicitly mentioned.

METHOD DETAILS

Surgery

Stereotaxic surgical procedures were used to inject opsins packaged in adeno-associated viruses (AAVs), neuronal tracers as previously described (Brown et al., 2012; O'Connor et al., 2015) or to implant bilaterally cannulas and optic fibers for *in vivo* experiments. In brief, isoflurane in 100% oxygen was used to induce and maintain anesthesia at 5% and 2%, respectively. Anesthetized mice were placed in a stereotactic frame (Stoelting; Illinois, USA) and underwent craniotomies. Graduated glass pipettes with a tip diameter of 10-15μm were filled with virus or neuronal tracer and lowered into the target region with substances injected at a rate of approximately 50-100nl/min. Pipettes were left in the injection site for about 5 min to let the virus or neuronal tracer diffuse. For implanting infusion cannulas or optic fibers, three screws were placed into the skull to anchor the mount. The mount was secured with dental cement (Lang Dental Manufacturing, Illinois, USA). Mice were let recover for at least one week following the surgery.

Channelrhodopsin injections

For *ex vivo* electrophysiology recordings requiring optogenetic neuronal excitation, AAV5-EF1A-DIO-ChR2(H134R)-eYFP was bilaterally injected (500nl/side) in mice expressing Cre under the D1 receptor promoter (D1Cre mice). Effectors were injected into NAcSh with coordinates (mm relative to Bregma): AP +1.5, ML ± 0.7, DV −4.4.

For *in vivo* high-frequency stimulation, the AAV-EF1A-DIO-ChETA-EYFP was bilaterally injected in the NAcSh using the same coordinates as above.

For experiments requiring selective recording of LH GABA or glutamate neurons, VGATCre (Stock No: 016962, The Jackson Laboratories, Main, USA; Bred in house) or VGluT2Cre mice (Stock No: 016963, The Jackson Laboratories, Main, USA; Bred in house) (respectively) were injected bilaterally (500nl/side) with AAV5-DIO-EF1A-mCherry in LH (AP −1.17, ML ± 1.17, DV −4.9) and AAV5-hsyn-ChR2(H134R)-eYFP in the NAcSh, as detailed above. For LH VGlut2 connectivity experiment, we injected AAV5-DIO-EF1A-tdTomato instead of AAV5-DIO-EF1A-mCherry. Recordings were performed approximately one month following injections to ensure expression of the construct. All viral constructs were purchased from UNC Vector Core, North Carolina, USA.

Infusion cannulas implantation

Wild-type mice were implanted bilaterally with infusion cannulas (7.5mm, C315GS-5/Spc; Bilaney Consultants, Düsseldorf, Germany) into the LH with a 10° angle at coordinates AP −1.2, ML ± 2.0, DV −4,57 from the brain surface). Dummys (7.5 mm, C315DCS-5/Spc, Bilaney) were used for maintaining the cannulas.

Optic fiber implantation

Optic fibers were constructed in house using using a 200 μM core, 0.39 NA multimode fiber (FT200UMT; Thor Labs, Dachau, Germany) coupled to a 1.25 mm OD ceramic zirconia ferrule (Precision Fiber Products, California, USA) following the procedure from Sparta et al. (2011) and were implanted into the LH at coordinates AP −1.2, ML ± 1.2, DV −4.6 in D1Cre mice previously injected with ChR2 in the NAcSh.

Neuronal tracing with CTB

D1rd1a-tdTomato mice (Stock No: 016204, The Jackson Laboratories, Main, USA; Bred in house) were injected with 250 nL of cholera-toxin subunit B (CTB) conjugated with different Alexa fluorophores (Thermo Fisher Scientific, Massachussetts, USA) in the following brain areas (all coordinates in mm relative to Bregma); LH: AP −1.17, ML −1.17, DV −4.9; VP: AP +0.6, ML −1.45, DV −4.9; VTA: AP −3.3, ML −0.5, DV −4.4; aLH: AP −0.2, ML −1.2- DV −4.9; pLH: AP −1.2, ML −1.2, DV −4.9. Eleven days after surgery, mice were injected with a lethal dose of pentobarbital and subject to intra-cardiac perfusion with 10mL PBS followed by 20 mL of 4% paraformaldehyde (PFA), once corneal and pinch reflexes were lost. Brains were removed, stored overnight in 4% PFA at 4°C and the following day 50 μm brain sections were cut on a vibrotome and mounted with fluorescent medium containing DAPI (AB104139; Abcam, Cambridge, UK).

Images of injection sites or entire sections were taken with an automated slide scanner (Axioscan.Z1; Zeiss; Oberkochen, Germany). For cell counting or high magnification images, a confocal laser-scanning microscope was used (LSM700; Zeiss), with images for CTB quantification in NAcSh obtained using a x40/1.3 NA oil objective (320 × 320 μm). In each experiment, laser power, gain, digital gain and offset values were maintained constant. For each mouse, two images (dorsal and ventral) per section were obtained at 4 different rostro-caudal coordinates of NAcSh, providing 8 images per mouse. Cell numbers or percentage values were averaged within a section for each mouse and then between mice for the final mean percentage value. Manual cell counting and colocalization analysis was performed using ImageJ (NIH).

Monosynaptic rabies tracing

The method used followed that described previously (O'Connor et al., 2015; Watabe-Uchida et al., 2012). In brief, Drd1a-tdTomato x VGlut2Cre mice (bred in house) were injected with 250-400 nL of AAV5-Flex-TVA-mCherry mixed with AAV8-Flex-RG unilaterally in the LH (AP −1.2, ML −1.2, DV −4.75). Fourteen days later 1 μL of SADΔG-EFG(EnvA) was injected in LH using the same coordinates. Seven days after this final injection, mice were perfused and brains processed for imaging and cell counting in NAcSh.

Whole-cell electrophysiology

Acute 200-250 μm coronal slices of NAcSh or LH were cut using a vibratome in ice-cold cutting solution based on artificial cerebrospinal fluid (ACSF) continuously bubbled with 95% O2 and 5% CO2 (carbogen). ACSF contained (in mM) 119 NACl, 2.5 KCl, 1.3 MgCl2, 1.0 NaH2PO4, 26.2 NaHCO3, 2.5 CaCl2 and 11 glucose. The cutting solution was prepared adding (in mM) 3 kynurenic acid, 26.2 NAHCo3, 225 sucrose, 1.25 glucose, 4.9 MgCl2 and 1.22 CaCl2 to the ACSF solution. Slices were kept in ACSF at 35°C for 15 min for recovery and then kept at room temperature until recordings. Once transferred in the recording chamber, the slice was superfused with 2.4 ml/min ACSF at physiological temperature (34°C) and continuously bubbled with carbogen.

For whole-cell recordings of inhibitory transmission, borosilicate glass pipettes (6-9 MOhm) were filled with an internal solution containing (in mM) 100 KCl, 30 potassium gluconate, 45 MgCl2, 10 sodium creatine phosphate, 3.4 Na2ATP, 0.1 Na3GTP, 1.1 EGTA and 5 HEPES. The reversal potential of Cl^- for the internal solution was −4.89 mV. Currents were amplified and filtered at 2.4 KHz, digitized at 10 KHz. Access resistances were monitored by a hyperpolarizing step of −4 mV every 10 s; the experiment was discarded if the access resistance was above 35 mΩ or changed by more than 20%.

For plasticity experiments in naive mice, D1Cre mice injected in the NAcSh with AAV5-DIO-EF1A-ChR2(H134R)-eYFP were used and recordings were made from non-identified LH cells with the anteroposterior coordinates between 0.7 mm and −1.70 mm from bregma.

When we selectively recorded from LH glutamate and GABAergic neurons, we used VGaTCre and VGlut2Cre mice injected with AAV5-hsyn-ChR2(H134R)-eYFP in the NAc and with AAV5-DIO-EF1A-mCherry or AAV5-DIO-EF1A-tdTomato in the LH. LH GABA or glutamate neurons in the acute slice preparation could be so identified by expression of mCherry or tdTomato.

Neurons were visualized with a 40x objective, with fluorescent neurons identified using appropriate filter sets. To activate the optogenetic effector, 2 pulses of 470 nm blue light (4 ms, 50ms inter-stimulus interval) were flashed through the microscope using an LED system (Product No: LEDD1A; Thorlabs, New Jersey, USA). Light-evoked inhibitory post-synaptic currents were monitored in the presence of 2mM kynurenic acid (Sigma Aldrich, Missouri, USA). The high-frequency stimulation (HFS) protocol comprised four stimulus trains of 100 light pulses (4ms pulse) repeated each 20 s apart. Where indicated, Foskolin (10 μM), WIN 55,212-2 (2 μM), SR141716A (5 μM) or SKF38393 (10 μM) were applied (all purchased from Tocris Biosciences, Bristol, UK). These compounds were dissolved in 100% Dimethyl Sulfoxide (DMSO, Sigma-Aldrich). The final DMSO dilution in ACSF was $1{:}10^4$. All recordings were conducted with interleaved timed controlled recordings. Recordings from control and drug-treated cells were interleaved in the same animal. Representative example traces are average of 30 consecutive sweeps. They show the last 5 min of baseline and the last 5 min of recording. Coefficient of variation ($1/CV^2$) was calculated from the averaged 30 sweeps at the end of the baseline period and end of the recording.

In vivo experiments

Unless otherwise stated, the following studies used D1Cre female and male mice (Stock No: 37156, The Jackson Laboratories, Main, USA; Bred in house) prepared with ChR2 in NAcSh, as described above. After recovery from surgery, and starting 3-5 days prior to the manipulation, animals were single-housed and provided *ad libitum* access to standard chow. Exact numbers of animals used for each experiment is provided in Tables S1–S3.

Acute food restriction (AFR)

To initiate acute food restriction, individually housed mice were transferred to a new cage without food, ensuring no food was hidden in the bedding material. Control animals were also transferred to a new cage but had *ad libitum* access to food throughout. The next morning, mice were prepared for *ex vivo* whole-cell patch clamp recordings, detailed above.

Plasticity after 7 days from AFR

Mice were subjected to the AFR protocol described above but slices were prepared after 7 days from the AFR. Body weight and food intake were measured before and after AFR, as well as one day before the recording and on the recording day itself.

Systemic delivery of CB1R antagonist

Mice were injected with the CB1R antagonist SR141716A (10mg/kg; injection volume of 1ml/kg; IP; Product No. 0923, Tocris Biosciences, Bristol, UK) or its vehicle (0.3% Tween80/Saline v/v). In AFR experiments, injections were given once just before lights off (ca. 1800h), which coincided with the start of AFR, and again the following morning, ca. 1h prior to preparation of acute brain slices for electrophysiology recordings (Figures 5A–5D) or prior to assessment of licking microstructure (Figures 5I–5M) described below. In high-fat experiments (detailed below), wild-type mice were injected once every 12h over the three-day period at ca. 2000h and 0800h.

Local infusion of CB1R antagonist/agonist

After one night of AFR and prior to the assessment of licking microstructure, wild-type mice were infused with the drug using a steel injector (7.5mm, C315IS-5/Spc, Bilaney) extending 0.5 from the tip of the implanted cannula. A tube (C232CGT, Bilaney) connected the steel injector to a 10 μL syringe (HA-80365 / 701 N; Hamilton, Bonaduz, Switzerland), which was driven by a pump (Pump 11 elite; Harvard Apparatus, Les Ulis, France) at a rate of 150 nL / min. The infusion system was filled with distilled water and separated from the infused drug by a small air bubble.

Mice were habituated to this procedure for two days before the test by connecting them to the empty infusion apparatus with a shortened steel injector to prevent damage to the tissue during the habituation phase. SR141716A was used at 1.5 μg per side and dissolved in 100% DMSO, based on previous report (Hu et al., 2015). Each mouse received separate infusions of the drug or vehicle (100% DSMO) with a week recovery between each infusion. To confirm cannula placements, mice were deeply anesthetized with chloral hydrate and infused with 100 nL per side of Chicago blue ink via the bilateral injector. After decapitation, brains were transferred into 4% paraformaldehyde (PFA) for overnight fixation at 4°C. Brain sections were cut at 100 μM on a vibrotome (Model VT1200s; Leica, Nunningen, Switzerland), mounted and visualized with an upright microscope (Zeiss Axiophot; Zeiss, Feldbach, Switzerland). For infusion of the CB1R agonist, the same procedures described above were used but mice were fed *ad libitum* all along the experiment.

Optogenetic HFS experiments

After one night of AFR and 15 min prior to the licking microstructure assessment (test), fiber optic cannulas of D1Cre mice were connected via patch chord (ThorLabs, Dachau, Germany) to a rotary joint (FRJ_1X2_FC-2FC; Doric Lenses, Quebec, Canada) suspended above a neutral cage. A second patch chord connected the rotary joint with a blue laser (SDL-473-100mW, Shanghai Dream Lasers; Shanghai, China). Laser power at the end of the patch chord was about 15-20 mW. At the tip of the optic fiber, we estimate laser power to be approximately 10-14 mW. Optogenetic HFS was then given at the frequency used *in vitro* (4ms pulses at 100 Hz repeated 4 times with 20 s ISI). Mice were habituated to the optogenetic apparatus before the optogenetic HFS.

To avoid any non-reversible effect of the optogenetic HFS, mice were first given mocked stimulation (optic fiber not connected) in the first test and optogenetic HFS at the second assessment. Once tests were completed, mice were sacrificed for confirmation of viral infection and optic fiber placement, which we reported on a schematic.

Assessment of licking microstructure for peripheral/local CB1R antagonist and HFS *in vivo*

Mice were trained to lick for a liquid fat solution (Lipofundin, Braun Medical, Switzerland; 5% v/v in water) during 1h daily sessions over three days and were *ad libitum* fed throughout training. Sessions were performed in a mouse operant box (15.9 × 14 × 12.7 cm; MedAssociate, Vermont, USA) equipped with a contact lickometer (ENV-250, MedAssociates). Recording of licks was achieved through MED-PC IV software and a custom code written in MED-State Notation (O'Connor et al., 2015). The recorded data allow analysis of licking microstructure. A lick/bout was defined as three or more consecutive licks with inter-lick interval < 1 s. After training, licking tests were conducted the morning following AFR, or with *ad libitum* feeding prior to control tests. In experiments where mice were repeatedly tested, each licking test was followed a week of recovery between tests (i.e., with *ad libitum* feeding) and mice were retrained in the operant boxes for 3 days prior to the subsequent test.

High fat diet exposure

Individually housed mice were provided access for 3 days to either high fat pellets (60% calories from fat; Product No: F3282, Bio-Serv, New Jersey, USA) or continued to receive standard chow. Body weights were recorded once daily throughout the experiment, at the same time each day. After three days of access to high-fat or chow, mice were prepared for *ex vivo* patch-clamp experiments. In experiments including CB1R antagonism (Figures 4E and 4F), wild-type mice were used and the quantity of high-fat diet consumed over three days was also recorded daily.

QUANTIFICATION AND STATISTICAL ANALYSIS

For assessing plasticity differences in electrophysiology, average IPSCs amplitudes from the last 5 min of recordings were compared between groups. Since groups comprised both male and female mice, body weight and food intake was normalized to baseline days to account for inherent body weight and food intake differences between male and female mice of the same age. For experiments involving two independent groups, unpaired, two-tailed Student t test was used. For experiments involving more than two groups or with repeated-measures, one or two-way ANOVA was used with between or within-subjects factors defined accordingly. Where significant main effects or interaction terms were found, further comparisons made by unpaired, two-tailed t test's. Bonferroni corrections were applied for multiple comparisons. Whenever assumption of sphericity was violated in within-subjects ANOVA, Greenhouse-Geisser correction was used. Statistical tests were performed using SPSS (IBM SPSS Statistics for Windows, Version 24.0. Armonk, NY: IBM Corp.), and the tests used are further detailed in the figure legends. All graphs show means, while error bars indicate standard error of mean (SEM).

Neuron, Volume *107*

Supplemental Information

Depression of Accumbal to Lateral Hypothalamic Synapses Gates Overeating

Sarah Thoeni, Michaël Loureiro, Eoin C. O'Connor, and Christian Lüscher

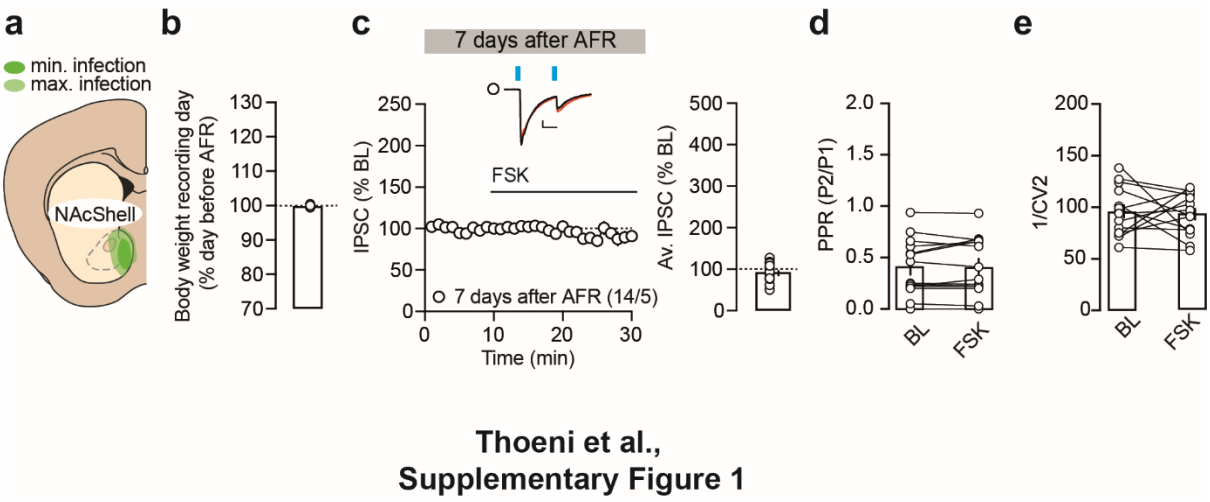

Figure S1. Related to Figure 1.FSK induced i-LTP is absent 7 days after an acute food restriction episode.

(**a**) Schematic representing the maximum and minimum infection with the AAV-DIO-ChR2 from animal that were kept in the study.
(**b**) Body weight from mice tested 7 days after a single 24h food restriction episode. Mice returned to their baseline weight.
(**c**) IPSC expressed as a percent of baseline (BL). Bath application of forskolin (FSK) was unable to potentiate the inhibitory transmission.
(**d**) PPR ratio was not changed by FSK.
(**e**) The coefficient of variation was not affected by FSK

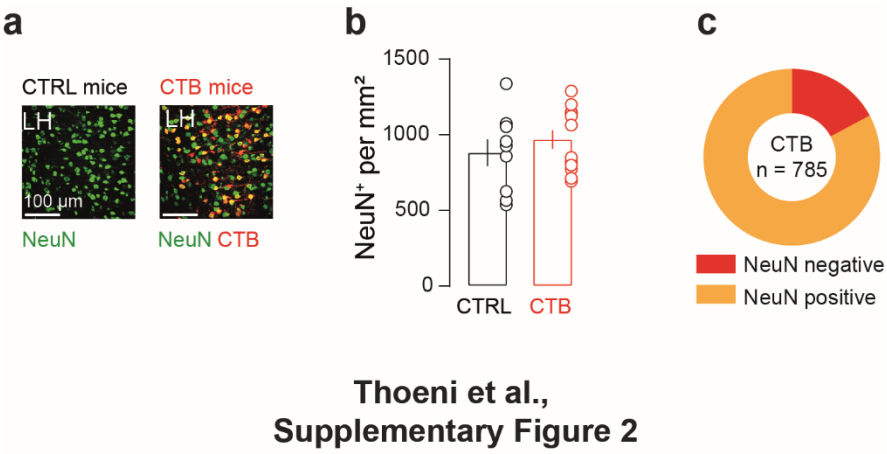

Figure S2. Related to Figure 2. Quantification of NeuN expression in mice injected with CTB in the LH.

(**a**) To control for CTB-induced lesion in the LH as a limitation of our strategy, we quantified the expression of NeuN in control or CTB-injected mice.
(**b**) NeuN expression density was similar in the LH of control and CTB-injected mice: $t(19) = 0.8260$, $p=0.4190$.
(**c**) 82.8% of CTB positive colocalized with NeuN, further demonstrating that CTB did induce a lesion in 10 days after the injection.
Plots show mean ± SEM.

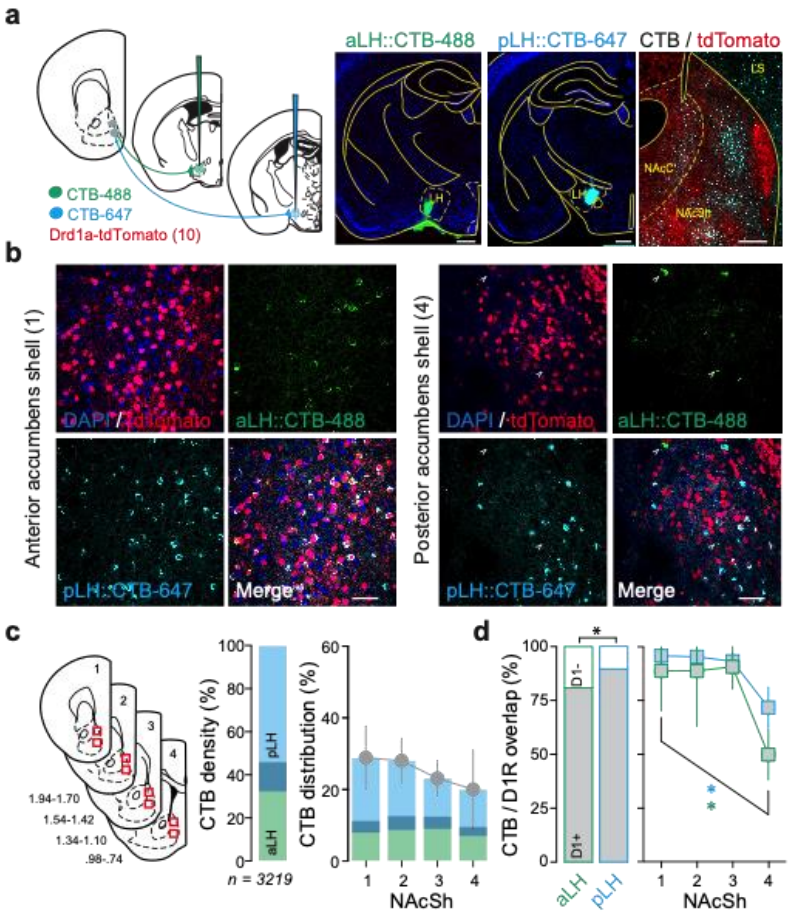

Figure S3. Related to Figure 2. Dual retrograde tracing from anterior and posterior lateral hypothalamus in Drd1a-tdTomato mice

(**a**) Schematic of experiment (left), with example images of Cholera toxin subunit-B (CTB) injection sites in anterior and posterior lateral hypothalamus (aLH/pLH) and CTB-labeled cell bodies visible in the nucleus accumbens. NAcC: accumbens core, NAcSh: accumbens shell, LS: lateral septum. All images are from the same animal. Scale bars: left & center: 500μm; Right, 200μm.

(**b**) From the animal in (A), confocal images from anterior (left) and posterior (right) NAcSh showing colocalization of CTB with tdTomato (i.e. D1R-MSNs). Arrowheads indicate non-colocalizing neurons located in posterior NAcSh. Scale bars: 50μm.

(**c**) Schematic indicating imaging sites across anterior/posterior NAcSh (left), with proportion of all CTB cells identified in NAcSh (n=3219) as aLH (green), pLH (light blue) or dual projecting (dark blue; center) and density distribution of each CTB type across NAcSh (right; grey points show group mean total CTB densities ± SEM).

(**d**) Proportion of all aLH or pLH projecting MSNs that colocalize with tdTomato (i.e. D1R-MSNs; left). Significantly fewer MSNs projecting to aLH vs. pLH were D1R+ (80.9 ± 3.51% vs. 89.5 ± 0.7%; paired t-test, *p < 0.05). Distribution of CTB/tdTomato overlap across anterior/posterior NAcSh (right). Significantly fewer MSNs located in the most posterior quarter of NAcSh and projecting to either aLH or pLH were D1R+ (area 1 vs. 4, Bonferroni corrected t-test, *p < 0.016).

Plots shows means ± SEM.

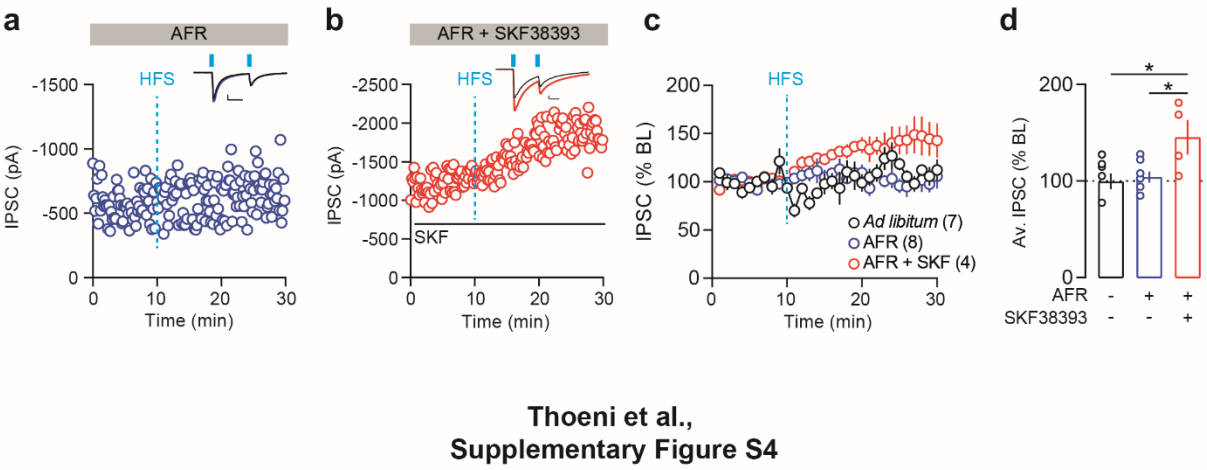

Thoeni et al.,
Supplementary Figure S4

Figure S4. Related to Figure 6. Ex vivo 100Hz high frequency optogenetic stimulation at D1-MSN to LH synapse.

(**a**) IPSC example recorded from a cell in the LH in food restricted mice. Stimulation occurred at 10 min.
(**b**) IPSC example recorded from a cell in the LH in food restricted mice. In this preparation, the D1 agonist SKF38393 was present in the bath during the entire recording.
(**c**) IPSC expressed as a percentage of baseline for all recorded cell from control, AFR and AFR + SKF38393 groups.
(**d**) Grouped IPSC. The IPSC was significantly increased in AFR mice when SKF38393 was bath applied. ANOVA: $F(2,16) = 4.073$, $p<0.05$. Post-hoc Bonferonni t-test: * $p<0.05$.

SUPPLEMENTARY TABLES

Experiment & Figure	Mouse line	Virus / Tracer	Injection site	n
CTB in LH and VP Fig. 2	Drd1a-tdTomato	CTB-Alexa488, CTB-Alexa567	LH, VP	5
CTB in LH and VTA Fig. 2	Drd1a-tdTomato	CTB-Alexa488, CTB-Alexa567	LH, VTA	6
Rabies tracing Fig.3	Drd1a-tdTomato X VGluT2Cre	AAV5-Flex-TVA-mCherry AAV8-Flex-RG SADΔG-EFG(EnvA)	LH	2
aLH and pLH Fig. S3	Drd1a-tdTomato	CTB-Alexa488, CTB-Alexa567	aLH, pLH	10

Table S1. Related to Figure 2 and Figure 3. Details of mice used in tracing experiments.

Experiment & Figure	Mouse line	Virus / Tracer	Injection site	n
HFS, FSK and Control cells Fig. 1	D1Cre	AAV5-EF1A-DIO-ChR2(H134R)-eYFP	NAcSh	22
FSK in the VP and Control cells Fig. 1	D1Cre	AAV5-EF1A-DIO-ChR2(H134R)-eYFP	NAcSh	5
FSK and Control cells Fig. 3	VGATCre	AAV5-hsyn-ChR2(H134R)-eYFP AAV5-DIO-EF1A-mCherry	NAc (Chr2) LH (mCherry)	6
LH VGlut2 connectivity Fig. 3	VGluT2Cre	AAV5-hsyn-ChR2(H134R)-eYFP AAV5-DIO-EF1A-tdTomato	NAcSh (ChR2) LH (TdTomato)	5
FSK and Control cells Fig. 3	VGluT2Cre	AAV5-hsyn-ChR2(H134R)-eYFP AAV5-DIO-EF1A-mCherry	NAc (Chr2) LH (mCherry)	6
Acute food restriction and FSK Fig. 1	D1Cre	AAV5-EF1A-DIO-ChR2(H134R)-eYFP	NAcSh	12
7 days after acute food restriction Fig. S1	D1Cre	AAV5-EF1A-DIO-ChR2(H134R)-eYFP	NAcSh	14
Acute food restriction and FSK in LH GABA cells Fig. 3	VGATCre	AAV5-hsyn-ChR2(H134R)-eYFP AAV5-DIO-EF1A-mCherry	NAc (Chr2) LH (mCherry)	12
Acute food restriction and FSK in LH glutamate cells Fig. 3	VGluT2Cre	AAV5-hsyn-ChR2(H134R)-eYFP AAV5-DIO-EF1A-tdTomato	NAcSh (ChR2) LH (TdTomato)	10
WIN55212-2 and Control cells in ad libitum fed mice Fig. 4	D1Cre	AAV5-EF1A-DIO-ChR2(H134R)-eYFP	NAcSh	16
Acute food restriction and CB1R antagonist on slice Fig. 4	D1cre	AAV5-EF1A-DIO-ChR2(H134R)-eYFP	NAcSh	15

Acute food restriction and CB1R antagonist Fig. 5	D1Cre	AAV5-EF1A-DIO-ChR2(H134R)-eYFP	NAcSh	32
High fat exposure Fig. 1 and 5	D1Cre	AAV5-EF1A-DIO-ChR2(H134R)-eYFP	NAcSh	16

Table S2. Related to Figure 1, Figure 3, Figure 4 and Figure S1. Details of mice used for whole-cell patch clamp recordings.

Experiment & Figure	**Mouse line**	**n**
Acute food restriction and systemic CB1R antagonist Fig. 5	C57BL/6J	14
High fat exposure and CB1R antagonist Fig. 5	C57BL/6J	15
Acute food restriction and HFS in vivo Fig. 6	D1cre	7
Local infusion of CB1R agonists and antagonist Fig. 5	C57BL/6J	12

Table S3. Related to Figure 5 and Figure 6. Details for the mice used for behavioural experiments.